The Geological Society of America
Special Paper 511
2015

The Shatsky Rise oceanic plateau structure from two-dimensional multichannel seismic reflection profiles and implications for oceanic plateau formation

Jinchang Zhang*
William W. Sager†
Department of Oceanography, Texas A&M University, College Station, Texas 77843, USA

Jun Korenaga
Department of Geology and Geophysics, Yale University, New Haven, Connecticut 06520, USA

ABSTRACT

The Shatsky Rise is one of the largest oceanic plateaus, a class of volcanic features whose formation is poorly understood. It is also a plateau that was formed near spreading ridges, but the connection between the two features is unclear. The geologic structure of the Shatsky Rise can help us understand its formation. Deeply penetrating two-dimensional (2-D) multichannel seismic (MCS) reflection profiles were acquired over the southern half of the Shatsky Rise, and these data allow us to image its upper crustal structure with unprecedented detail. Synthetic seismograms constructed from core and log data from scientific drilling sites crossed by the MCS lines establish the seismic response to the geology. High-amplitude basement reflections result from the transition between sediment and underlying igneous rock. Intrabasement reflections are caused by alternations of lava flow packages with differing properties and by thick interflow sediment layers. MCS profiles show that two of the volcanic massifs within the Shatsky Rise are immense central volcanoes. The Tamu Massif, the largest (~450 km × 650 km) and oldest (ca. 145 Ma) volcano, is a single central volcano with a rounded shape and shallow flank slopes (<0.5°–1.5°), characterized by lava flows emanating from the volcano center and extending hundreds of kilometers down smooth, shallow flanks to the surrounding seafloor. The Ori Massif is a large volcano that is similar to, but smaller than, the Tamu Massif.

*Now at Key Laboratory of Marginal Sea Geology, South China Sea Institute of Oceanology, Chinese Academy of Sciences, Guangzhou, 510301, China, *and* Key Laboratory of Marine Mineral Resources, Ministry of Land and Resources, Guangzhou, 510075, China.
†Now at Department of Earth and Atmospheric Sciences, University of Houston, Houston, Texas 77204, USA.

Zhang, J., Sager, W.W., and Korenaga, J., 2015, The Shatsky Rise oceanic plateau structure from two-dimensional multichannel seismic reflection profiles and implications for oceanic plateau formation, *in* Neal, C.R., Sager, W.W., Sano, T., and Erba, E., eds., The Origin, Evolution, and Environmental Impact of Oceanic Large Igneous Provinces: Geological Society of America Special Paper 511, p. 103–126, doi:10.1130/2015.2511(06). For permission to copy, contact editing@geosociety.org.

The morphology of the massifs implies formation by extensive and far-ranging lava flows emplaced at small slope angles. The relatively smooth flanks of the massifs imply that the volcanoes were not greatly affected by rifting due to spreading ridge tectonics. Deep intrabasement reflectors parallel to the upper basement surface imply long-term isostasy with the balanced addition of material to the surface and subsurface. No evidence of subaerial erosion is found at the summits of the massifs, suggesting that they were never highly emergent.

INTRODUCTION

Oceanic plateaus are extensive undersea mountains often rising thousands of meters above the surrounding seafloor, with areas as large as millions of square kilometers and volumes as much as millions of cubic kilometers (Coffin and Eldholm, 1994). Many are large basaltic volcanic edifices with anomalously thick crust, implying extraordinary fluxes of magma from the mantle to the lithosphere (Coffin and Eldholm, 1994; Ridley and Richards, 2010). Thus, plateau formation can be an important indication of regional tectonic events and mantle behavior.

Oceanic plateaus are broad volcanoes with shallow slopes of only ~1°–2° or less (Coffin and Eldholm, 1994). In spite of similar compositions, they differ in size and morphology from the numerous smaller volcanic seamounts, which are characterized by steeper slopes (~5° or greater) (Smith, 1988). Plateau formation is poorly understood, and several mechanisms have been proposed. One class of proposed mechanisms envisions decompression melting of fertile upper mantle material at plate boundaries or cracks in the plates, such as leaky transform faults (Hilde et al., 1976), spreading ridge reorganizations (Anderson et al., 1992; Foulger, 2007), and/or weaknesses in the lithosphere caused by changes in plate stress (Saunders, 2005). However, it is difficult to explain the huge volumes of magma required for building large oceanic plateaus with these mechanisms (e.g., Coffin and Eldholm, 1994). An alternate explanation is the mantle plume hypothesis. Many think that oceanic plateaus form when the voluminous rising head of a nascent mantle plume arrives at the base of the lithosphere (the plume head hypothesis) (Richards et al., 1989; Mahoney and Spencer, 1991; Duncan and Richards, 1991; Coffin and Eldholm, 1994). Although this model is widely accepted and can explain some features of oceanic plateaus, there are notable exceptions. For example, rocks recovered from the main Shatsky Rise volcanoes are similar to mid-ocean ridge basalts in geochemistry and isotopic signatures, whereas most plume head models imply that lower mantle material is carried to the surface (Mahoney et al., 2005; Sager, 2005). A third suggested formation mechanism is cosmic, i.e., that plateaus are the result of a large meteorite impact (Rogers, 1982; Ingle and Coffin, 2004); the lack of evidence linking plateaus and impacts has led to limited acceptance of this hypothesis.

Among oceanic plateaus, the Shatsky Rise is unusual for oceanic plateaus because it has characteristics that fit both the mantle plume and plate edge hypotheses (Sager, 2005). Magnetic lineations show that it formed at a triple junction (Nakanishi et al., 1999), thus its formation is linked to plate boundaries. Moreover, the morphology of the Shatsky Rise suggests that it began forming with an enormous eruption, followed by lesser eruptions, as could be expected of the transition between plume head and plume tail (Sager and Han, 1993; Sager et al., 1999; Sager, 2005). The Shatsky Rise was drilled during Integrated Ocean Drilling Program (IODP) Expedition 324 (Sager et al., 2010), but its structure is still poorly known because it has not been imaged by modern deep-penetration seismic data. The seismic vessel R/V *Marcus G. Langseth* visited the Shatsky Rise on two cruises to acquire new marine seismic data. During one of these cruises, wide-angle seismic refraction data were collected over the southern Shatsky Rise (see Korenaga and Sager, 2012). Deeply penetrating two-dimensional (2-D) multichannel seismic (MCS) reflection profiles were collected on both cruises over the southern half of the rise, and these data allow us to image the structure of the plateau with unprecedented detail. In this article we describe the upper crustal structure of the Shatsky Rise using the MCS profiles and discuss implications for oceanic plateau formation. Based on morphology, it has been suggested that the Shatsky Rise is mostly made up of three large central volcanoes (Sager et al., 1999), a hypothesis that can be tested with the new MCS data. In Sager et al. (2013), this issue was addressed for the largest edifice (Tamu Massif; Fig. 1) and it was concluded that it is a single volcano. Here we expand upon this work with a larger set of observations and interpretations.

Geologic Background

The Shatsky Rise is located in the northwest Pacific Ocean, ~1600 km east of Japan (Fig. 1). It has dimensions of ~450 km × 1650 km and has an area equivalent to Japan or California. Its summits reach 2000–3000 m depth and it is surrounded by regional seafloor of 5500–6000 m depth. The Shatsky Rise consists of three bathymetric highs, the Tamu, Ori, and Shirshov massifs, as well as a low ridge, the Papanin Ridge, arranged on a southwest-northeast trend (Fig. 1). The plateau has an estimated volume of 4.3×10^6 km^3 (Sager et al., 1999), but the original size may have been even larger because it was formed at a ridge-ridge-ridge triple junction (Nakanishi et al., 1999) and part may have been carried away on other plates that are now subducted.

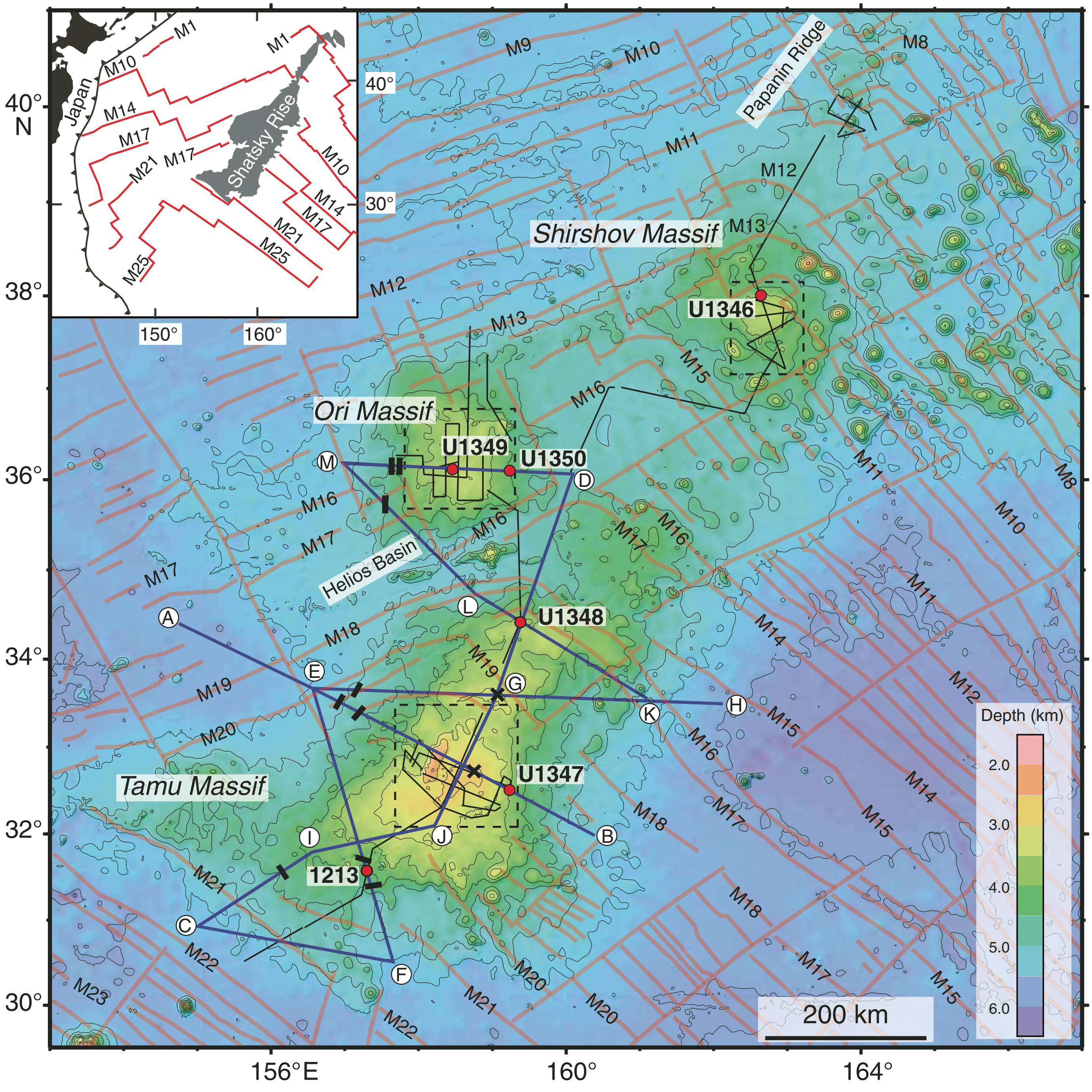

Figure 1. Bathymetry and tectonic map of the Shatsky Rise with seismic track lines. Bathymetry is from satellite-predicted depths with 500 m contours (Smith and Sandwell, 1997). Heavy red lines show magnetic lineations with chron numbers labeled for reference (Nakanishi et al., 1999). Heavy blue lines show multichannel seismic (MCS) reflection profiles collected by R/V *Marcus G. Langseth*. Letters next to seismic lines identify end points of MCS profiles for reference. Thin black lines show seismic reflection profiles collected during cruise TN037 (Klaus and Sager, 2002). Filled red circles show locations of the Ocean Drilling Program and Integrated Ocean Drilling Program drill sites mentioned in the text. Inset depicts the location of the Shatsky Rise relative to Japan and nearby subduction zones (toothed lines) and the wider magnetic lineation pattern. Heavy black tick marks show the locations of large down-to-basin faults seen on the MCS profiles. The fault strikes are estimated from multibeam bathymetry. The locations of summit calderas are indicated by × symbols. Dashed black boxes denote the summit areas of the three massifs shown in summit basement morphology maps in Figure 13.

Moreover, the total output of the mantle source may have been significantly greater if both the Shatsky Rise and the Hess Rise were formed from the same source, as suggested by Bercovici and Mahoney (1994).

The Shatsky Rise is at the junction of two magnetic lineation sets, the Japanese and Hawaiian lineations, which can be traced between the bathymetric highs (Fig. 1; Larson and Chase 1972; Hilde et al., 1976; Nakanishi et al., 1999). The age of ocean floor is younger toward the northeast from magnetic chron M21 (149 Ma), located at the southwest end of the Shatsky Rise, to M1 (126 Ma) at the northeast end (Fig. 1; Nakanishi et al., 1999; using the time scale of Gradstein et al., 2004). The Tamu Massif is the largest (~450 × 650 km) and oldest (ca. 145 Ma) volcanic edifice among the three bathymetric highs, and if it is a single volcano, it may be the largest single volcano on Earth (Sager et al., 2013). It apparently began to form around M21–M20 time (149–147 Ma) (Nakanishi et al., 1999, this volume). Prior to that time, the Pacific-Izanagi-Farallon triple junction moved northwest relative to the Pacific plate, but at about M21 time, it jumped ~800 km to the location of the Tamu Massif (Nakanishi et al., 1999). Basalts cored from Ocean Drilling Program (ODP) Site 1213, on the south flank of the Tamu Massif, yielded a radiometric age of 144.6 ± 0.8 Ma (Mahoney et al., 2005), which is near that of the magnetic lineations that surround the massif and consistent with the idea that the volcanic edifice formed near the triple junction (Nakanishi et al., 1999; Sager, 2005). Subsequently, the triple junction drifted northeast along the axis of the rise, and the three volcanic massifs and the Papanin Ridge were created in its path. Although individual massifs may have formed rapidly (Sager and Han, 1993), the span of magnetic anomalies associated with the Shatsky Rise implies that it took ~21 m.y. for the entire plateau to form.

Because the Shatsky Rise region on the Pacific plate has never been close to continental sediment sources, the plateau is covered by a mostly thin layer of pelagic sediments. Sediments deposited on the flanks are typically several hundred meters or less in thickness (Houtz and Ludwig, 1979; Ludwig and Houtz, 1979), whereas sediment caps at the summits are as much as ~1 km in thickness (Karp and Prokudin, 1985; Khankishiyeva, 1989; Sliter and Brown, 1993; Sager et al., 1999). The sediments on top of the rise are mostly composed of Cretaceous pelagic carbonates that were deposited above the calcite compensation depth (Sliter and Brown, 1993).

Basaltic basement rocks from the Shatsky Rise were recovered at ODP Site 1213 (Shipboard Scientific Party, 2002; Koppers et al., 2010) and at IODP sites U1346, U1347, U1349, and U1350 (Sager et al., 2010, 2011) (Fig. 2). ODP and IODP coring recovered tholeiitic basalts both as pillow lavas and massive flows, the latter as thick as ~23 m. The pillow lavas are associated with volcanic eruptions at modest effusion rates (Ballard et al., 1979), whereas the massive flows occur at high effusion rates and are characteristic of flood basalt provinces (Jerram and Widdowson, 2005; Bryan et al., 2010). Often the massive flows and pillow basalts are intercalated (Fig. 2). The thickest massive flows are found on the Tamu Massif at Sites 1213 and U1347. Massive flows also occur on the Ori Massif at Sites U1349 and U1350 and on the Shirshov Massif at Site U1346, but they are thinner and less common as the percentage of cored section composed of massive flows decreases from the Tamu to the Ori and Shirshov massifs. This shift implies a change from high effusion rates at the Tamu Massif to lower rates for the smaller edifices, suggesting that an initial burst of magmatic activity was followed by waning igneous output. It is interesting that interflow sediments are intercalated with igneous material composing the basaltic basement at Sites 1213, U1347, and U1350 and thick volcaniclastics make up significant portions of the cored igneous sections at Sites U1348 and U1349. Although some of these volcaniclastic sediments likely occur during the emplacement of lava flows, other such layers may exist because of explosive volcanism occurring in shallow water (Sager et al., 2010). The Site U1348 section is an example of shallow-water explosive volcanism and it implies that volcaniclastic formation is a significant part of plateau volcanism and that many basement highs consist of this type of material (Sager et al., 2011).

Seismic Data

Seismic data collected over the Shatsky Rise are scarce. Deep seismic refraction studies by Den et al. (1969) and Gettrust et al. (1980) both developed velocity-depth models, but neither was able to record the Moho discontinuity beneath the thickest part of the plateau, and the results are somewhat unreliable because of the now-outdated techniques used. Refraction lines across the center of the Tamu Massif were collected, and a maximum crustal thickness of ~30 km was reported (Korenaga and Sager, 2012).

Most seismic reflection data from the Shatsky Rise consist of old, low-resolution single channel profiles, which are not useful for investigating the subsediment structure. A number of 2- and 3-fold MCS reflection profiles over the Shatsky Rise were acquired on cruise TN037 in 1994 (Klaus and Sager, 2002), and some of these profiles were published (in Sager et al., 1999). Although these profiles usually show the interface between sediment and underlying igneous rocks (the igneous basement surface), they rarely display significant penetration below the igneous basement owing to the small sound sources used to collect these data. Thus, the TN037 data are useful for tracing igneous basement, but not for examining the subbasement structure.

DATA AND METHODS

Deeply penetrating 2-D MCS reflection data were collected from the R/V *Marcus G. Langseth* during cruise MGL1004 in 2010 and cruise MGL1206 in 2012. The seismic source was a 36-airgun array of 6600 in^3 (108.2 L) volume. The MCS lines were run with a 50 m shot spacing. The receiving array was a single, 6-km-long, 468 channel streamer with a 12.5 m group interval. With the ship speed used during both cruises, the seismic records had a nominal fold of 59. The common depth point interval was 6.25 m and the raw data were sampled at a rate of 2 ms and filtered to a frequency range of 2–206 Hz. In total, ~3350 km of MCS reflection lines were acquired (Fig. 1). ProMAX (version 2003.19.1) software was used for MCS processing. Processing steps included geometry setup, trace edit, band-pass filter, deconvolution, velocity analysis, normal moveout, stack, time migration, and automatic gain control.

The MCS lines crossed one ODP drill site (Site 1213) and four IODP drill sites (Sites U1347, U1348, U1349, and U1350) (Fig. 1), providing the opportunity to compare seismic data with cores and logs from the drill sites. This comparison allowed us to document the response of the seismic system to volcanic lithology, providing a basis for geologic interpretation of the seismic lines. Using core and log velocity and density data, synthetic seismograms were generated using Kingdom Suite

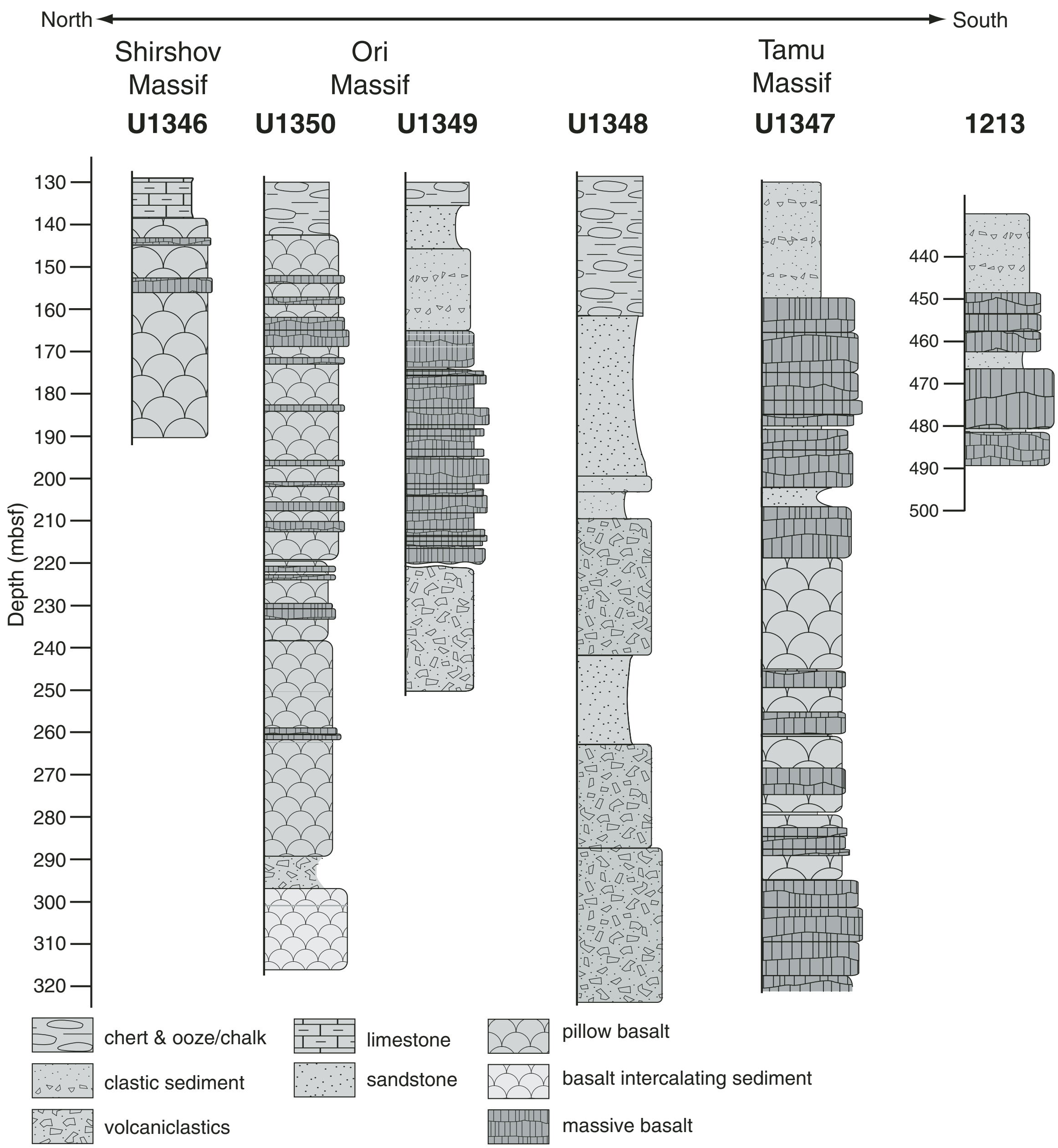

Figure 2. Lithology of cored igneous sections from the Shatsky Rise. Sites are arranged in order from northeast (left) to southwest (right) and depths have been shifted to align the tops of the igneous sections. Data from Sites U1346–U1350 are from Integrated Ocean Drilling Program Expedition 324 (Sager et al., 2010, 2011) and data from Site 1213 are from Ocean Drilling Program Leg 198 (Shipboard Scientific Party, 2002; Koppers et al., 2010). Site locations are shown in Figure 1.

(version 8.5) seismic interpretation software for comparison with seismic data from the field. Continuous velocity and density data from downhole logs are available only for sites U1347 and U1348, so these are the only sites for which we could calculate synthetic seismograms. The velocity and density data from core samples at other sites are too sparse for reliable synthetic computation. In addition, because IODP logging occurs with the drill string buried 80–100 m deep within the sediment section, the seafloor response of the logging data is usually not available because that section is shielded by pipe (Sager et al., 2010). Thus, the Expedition 324 logging data for sites U1347 and U1348 do not have the complete velocity and density curves from the seafloor down to the bottom of the holes. Therefore, it is not possible to match synthetics and seismic traces at the seafloor. The clearest signal in the log data occurs at the upper surface of the igneous section, so we used the top of the igneous section, instead of seafloor, to match waveform and amplitude between synthetics and seismic traces.

Kingdom Suite was also used to interpret the MCS reflection profiles. Using standard seismic stratigraphy techniques (Mitchum et al., 1977), seismic horizons were correlated and interpreted in geologic terms. Our particular focus was on layering within the part of the seismic section thought to represent igneous rock.

Assuming an average velocity for sedimentary layers of 2000 ms^{-1} and a water column velocity of 1500 ms^{-1}, we constructed maps of summit basement depths for the three massifs of the Shatsky Rise to learn about volcanic summit morphology. This plot was constructed using the *Marcus G. Langseth* MCS data as well as the seismic reflection profiles from cruise TN037 (Sager et al., 1999).

RESULTS

The new high-quality deep penetration MCS reflection data generally do a good job at imaging the upper crustal structure and layering of the Shatsky Rise. Features within the plateau are visible seismically because of impedance contrasts between layers with differing physical properties. The transition between sediments and igneous rocks frequently generates a high-amplitude reflection that can be interpreted as the top of the igneous basement. The igneous basement surface in our data set is mostly continuous and can be easily recognized because it often gives a strong reflection and is more irregular than smoother reflections above, which are interpreted as sediment layers. Within the uppermost igneous basement, layers interpreted as lava flow sequences can be identified by piecewise-continuous and subparallel intrabasement reflections. Piecewise-continuous reflections are reflector series that can be connected to infer longer reflectors. Typically individual segments are 5–20 km in length, but can be connected into reflectors several times that length. Another term for such reflectors is semicontinuous (e.g., Inoue et al., 2008). In addition, faults can be identified by offsets of strata or lateral terminations or breaks of layering.

Synthetic Seismograms

Calculation of synthetic seismograms from core and log velocity and density data shows the correlation of the lithology to the seismic reflections, giving a basis for geologic interpretation. In general, cored igneous sections on the Shatsky Rise are short, ranging from ~50 to 175 m in length, but the core data have high vertical resolution on the order of centimeters. Because of the low frequency of the seismic sound source (6–60 Hz with a peak at ~30 Hz; Vuong et al., this volume), the average wavelength for the sonic waves is tens of meters (~50–100 m assuming 30–60 Hz for a velocity of 4 kms^{-1}), so it is only possible to constrain several wavelengths of the subbasement seismic record using core and log data.

At Site U1347 on the upper eastern flank of the Tamu Massif, the ~160-m-thick igneous section shows that massive basalts are overlain by clastic sediments, intercalated with pillow basalts, and interbedded with interflow sediments (Fig. 3). The interface between the sediments and igneous basement (~90 m depth in Fig. 3) shows an abrupt rise in both velocity and density, generating a strong reflection identified as the top of the igneous basement.

Interflow sediment layers apparently account for several other reflections. Expedition 324 shipboard scientists described 4 significant sediment layers in the section (Roman numerals in Fig. 3), 3 of them ~4–5 m thick (Sager et al., 2010). Only one of these layers was recovered well and thus appears prominently in the graphic lithology (at 135 m depth in Fig. 3). Thicknesses for the other three sediment layers were inferred from the log data, which show 4 prominent low velocity-density horizons at ~115 m, 130 m, 180 m, and 200 m (Sager et al., 2010). The upper three lows are likely a result of sediment layers. The lowermost low is broader than the sediment layer (unit XIII in Fig. 3) and probably occurs because of higher porosity pillow flows and interflow debris. Impedance contrasts caused by these low velocity-density zones appear to cause the second positive signal peak (at ~130 m in Fig. 3) and the underlying broad negative (170–210 m). The lowest positive reflection occurs at the transition between pillow flows and thick massive flows, apparently caused by the slight increase in velocity and consistently high velocity and density values of the massive flows. At ~190 m depth there is a mismatch between the synthetic traces, which show a strong positive peak, and the field data, which do not. Here it appears that a narrow spike in the velocity and density log data generate a reflector in the synthetic data that is not matched in the field data. This mismatch may be a result of the difference in vertical resolution of the two data types.

The synthetic seismogram from Site U1348 (northern Tamu Massif) shows a variety of different sediments that exhibit multiple changes in velocity and density, resulting in many reflections in the synthetic section (Fig. 3). This section also shows a strong reflector at the top of the igneous section owing to an abrupt rise in velocity and density. Within the section, there is not always a clear correspondence between lithologic layers and seismic response. Although some of the modeled reflections obviously follow changes in lithology (e.g., the strong reflector at the base of the clastic sediment layer at ~50 m depth in Fig. 3), other reflections occur from velocity and density changes within a layer classified as a single lithology. Thus, in volcaniclastic sections the correlation between lithology and seismic layering can be complex.

In enlargements of MCS profile sections crossing Sites 1213, U1347, U1348, U1349, and U1350 (Fig. 4), the high-amplitude basement reflector can be easily identified because of its strong amplitude and because it often separates rough basement from smoother sediment layers. Basement reflectors are continuous and parallel to the seafloor. Intrabasement reflectors are not usually as continuous as the basement reflector. Although some shallower intrabasement reflectors are relatively continuous and parallel to the basement surface, most are rugged, irregular, and show scattering. Intrabasement reflectors appear to be piecewise-continuous and the pattern can be traced for longer distances. In general, the intrabasement reflectors are subparallel to the basement surface.

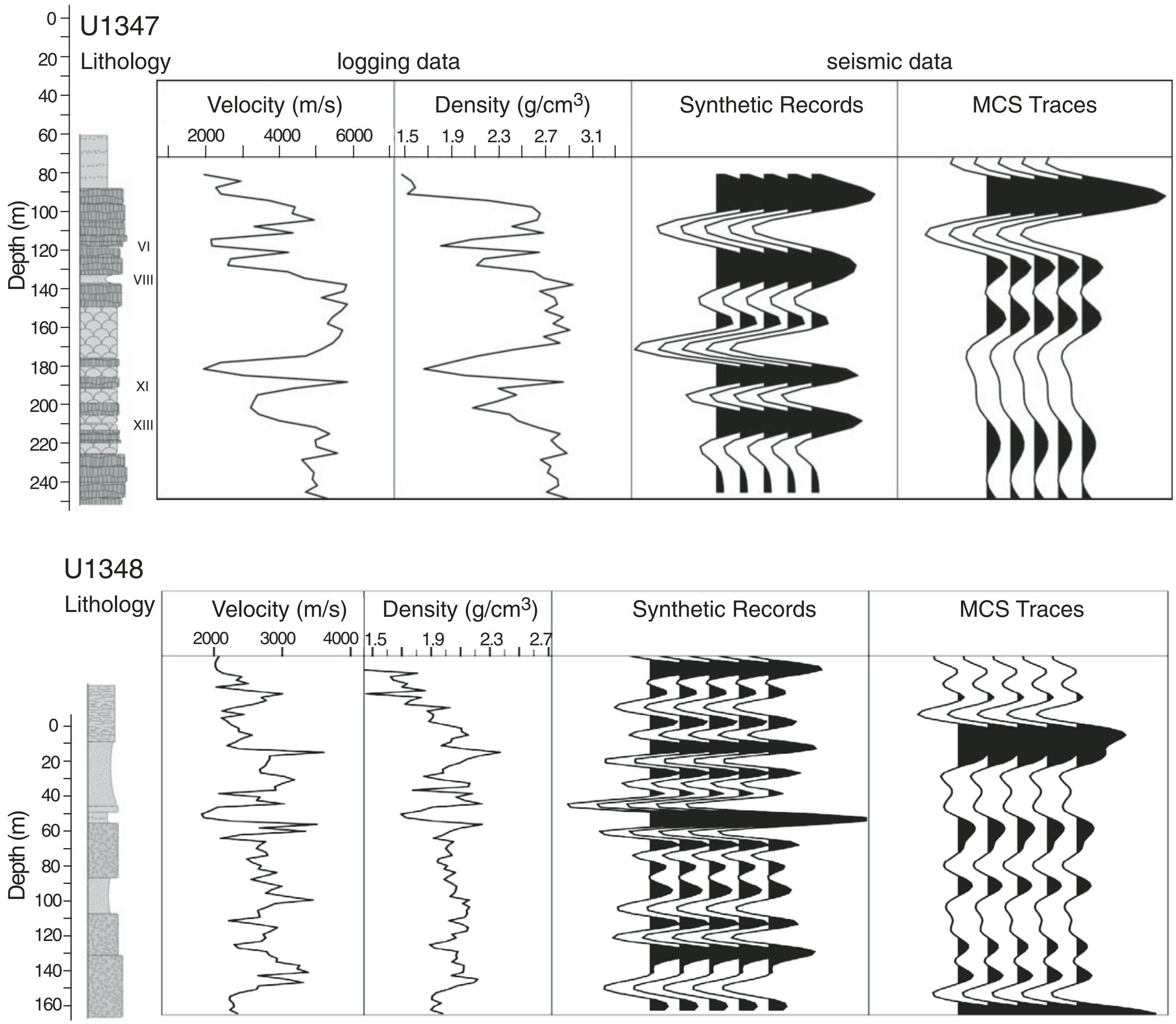

Figure 3. Synthetic seismograms of Integrated Ocean Drilling Program Sites U1347 (top) and U1348 (bottom) on Tamu Massif. The left panel shows lithologic description (Sager et al., 2010) and columns have been shifted in depth to align the top of the igneous sections in both logging and core data. Roman numerals denote sediment layers discussed in text. The middle two panels show velocity (ms^{-1}) and density ($g\ cm^{-3}$) curves from logging data (Sager et al., 2010). The right two panels show synthetic records and actual multichannel seismic (MCS) traces from field data. Synthetic and MCS traces are matched at the top of the igneous section.

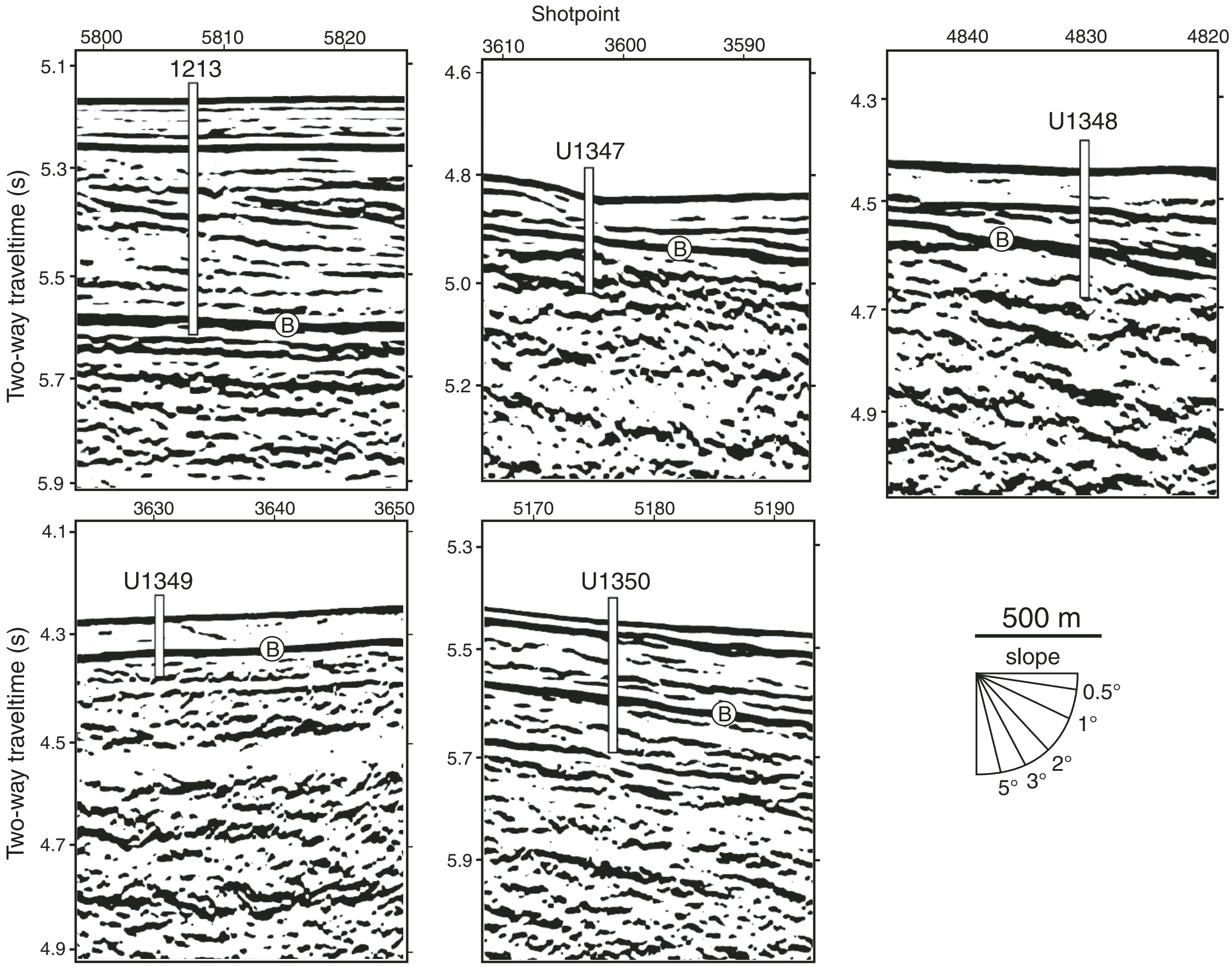

Figure 4. Enlargements of seismic sections across Ocean Drilling Program Site 1213 and Integrated Ocean Drilling Program Sites U1347, U1348, U1349, and U1350. The igneous basement surface is labeled in circled letter B. The vertical white bars with black border show the positions and depths of the drilled holes. Slope indicator applies to the seafloor and is calculated from vertical exaggeration of 22:1 using water velocity of 1500 ms^{-1}.

No matter whether the drill sites are located at the summits or on the flanks of the Shatsky Rise (Fig. 1), all of the crossing short seismic sections (Fig. 4) show that the slopes of seafloor are shallow (<0.5°). Although it is not possible to measure the true slope from widely spaced 2-D seismic lines because profile orientation relative to the maximum dip axis is unknown, the apparent slope is so shallow that the apparent dip is not greatly different from actual dip. The slope indicator in Figure 4 and other seismic sections (calculated from the vertical exaggeration using 1500 ms^{-1}) is strictly valid only for the seafloor, but where underlying layers are parallel to each other (i.e., layers have constant thicknesses), their velocity gradients in depth do not change the apparent slope, which means that the slopes of the subseafloor layers are the same as the slope of the seafloor. This applies to many of the Shatsky Rise profiles because basement and intrabasement reflectors are often parallel or subparallel to the seafloor (Fig. 4). Therefore, the slopes of basement and intrabasement reflectors would be nearly identical to the slope of the seafloor.

Tamu Massif

Line A-B (Fig. 5) is a complete profile across the southwest-northeast axis of the Tamu Massif. It displays the shallowest parts of the massif and shows many of its characteristic features. Beneath a thin blanket of sediment (except at the summit), the igneous basement reflector is easily traced across the plateau. This reflector exhibits a shallow slope, starting from ~1°–1.5° on the upper flanks to <0.5° on the distal lower flanks. The volcanic

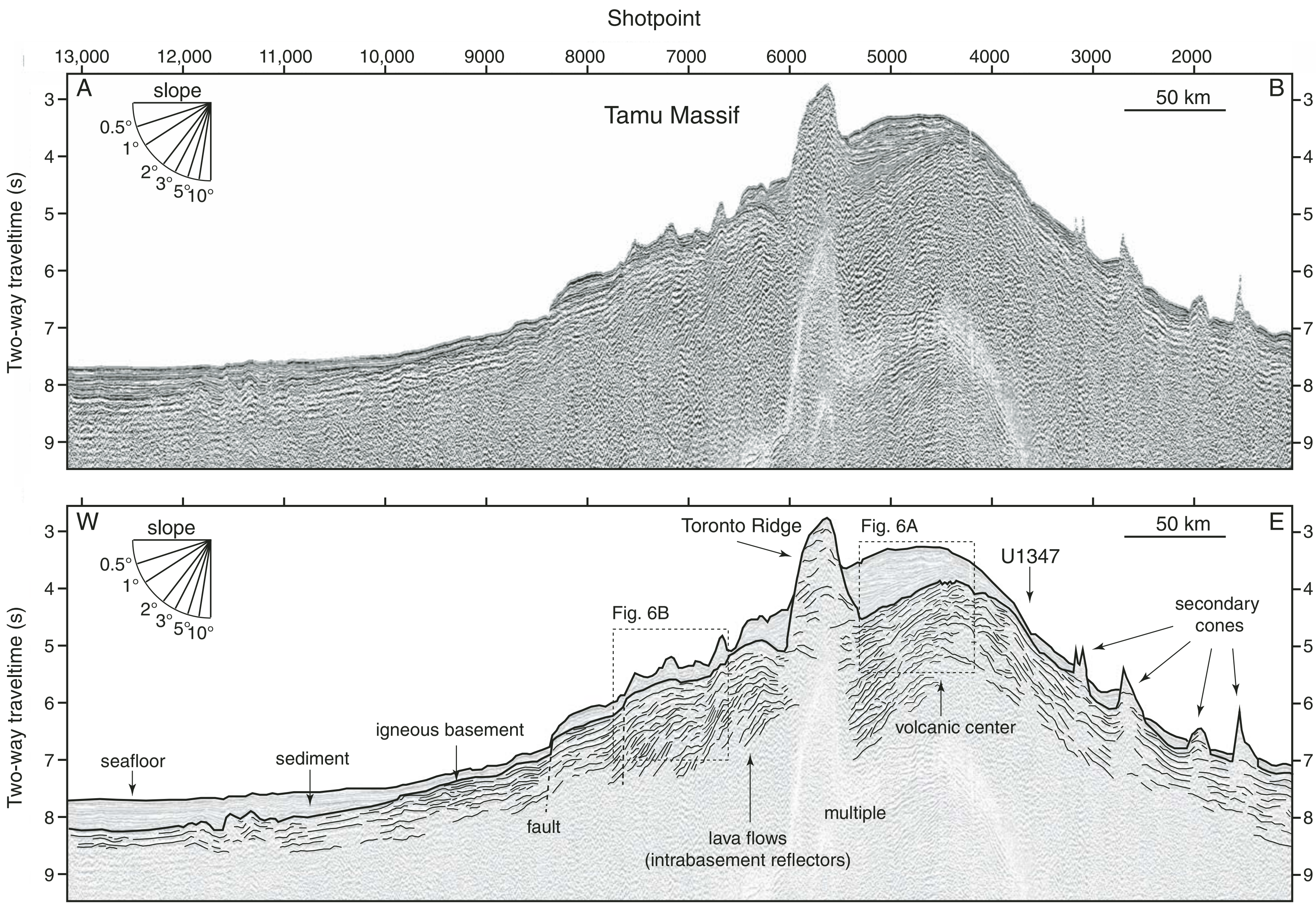

Figure 5. Multichannel seismic (MCS) reflection profile of line A-B, modified from Sager et al. (2013). Top panel shows uninterpreted MCS data, whereas bottom panel shows interpreted seismic section. The heavy black horizon represents the sediment-basalt interface (igneous basement). Thin dark lines represent selected intrabasement reflectors (lava flows) (Note that for clarity, not all intrabasement reflectors are highlighted in this and other large scale figures). Dashed lines represent faults. The arrow labeled U1347 shows the position of that drill site. Slope indicator refers to the seafloor (vertical exaggeration = 37:1). Dashed boxes highlight the enlarged segments shown in Figure 6.

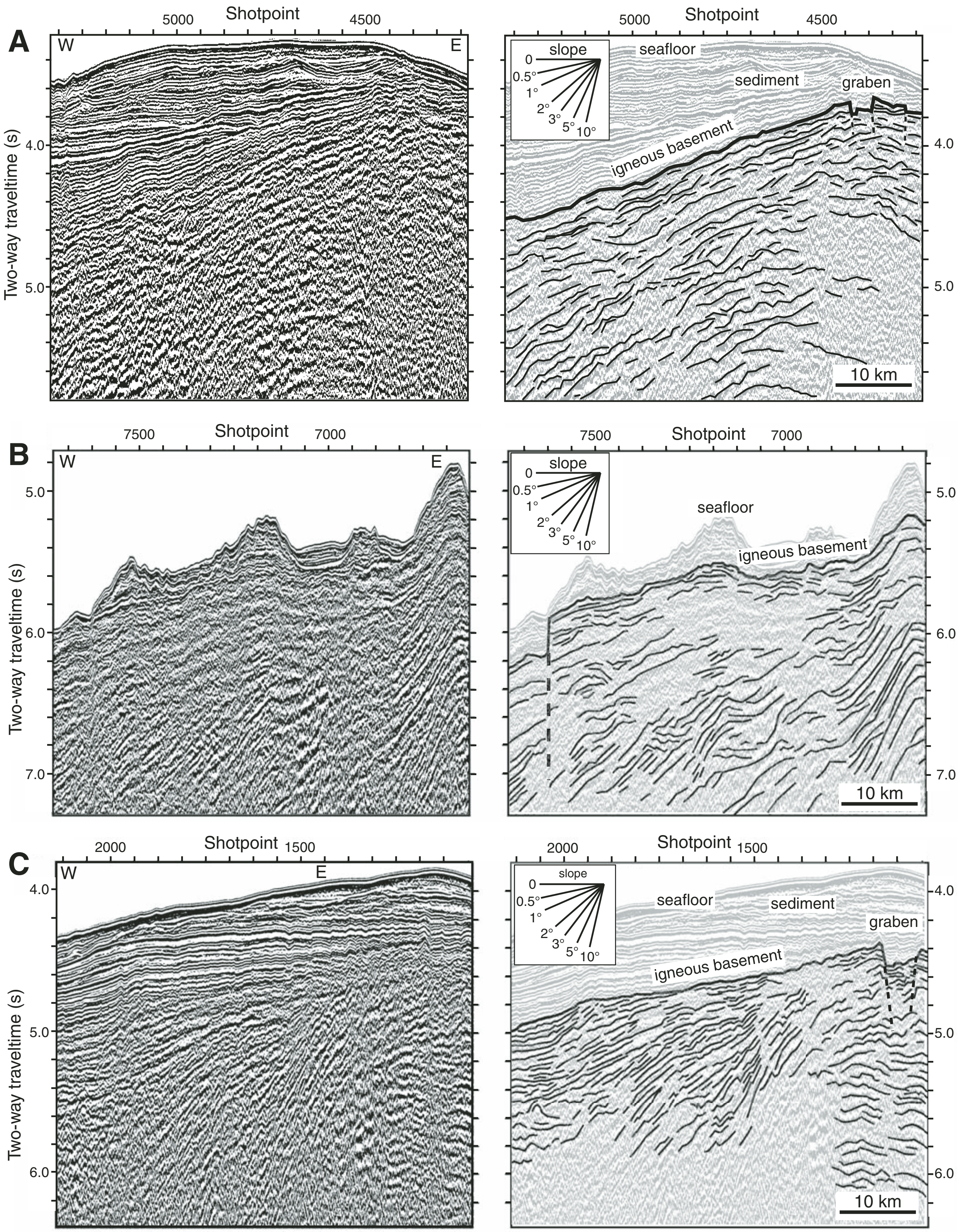
A
B
C
Shotpoint
W
E
Two-way traveltime (s)
slope
0
0.5°
1°
2°
3°
5°
10°
seafloor
sediment
graben
igneous basement
10 km

profile is symmetric across a rounded basement summit at shotpoint (SP) 4400 (Fig. 5). Numerous intrabasement reflectors are observed 0.5–2.0 s in two-way traveltime (TWTT) into the igneous pile (1000–4000 m subbasement depth assuming a sonic velocity of 4000 ms^{-1}). Individual intrabasement reflectors are piecewise-continuous and can be traced continuously to tens of kilometers in length, but the pattern continues hundreds of kilometers down the flanks. These reflectors are generally subparallel and follow the shallow slopes down the flanks, apparently imaging flow packages emanating from the volcanic center at SP 4400. Intrabasement reflectors continue the symmetric, domed shape of the eruptive center at depth, implying a long-term stability in relative location.

To illustrate intrabasement reflectors, two enlargements from line A-B are shown in Figure 6. Figure 6A, near the Tamu Massif summit, shows that the intrabasement reflectors are variable in continuity. Many can be traced for a few kilometers and some for tens of kilometers or more. Often several reflectors can be connected as a single horizon (i.e., piecewise-continuous). Many intrabasement reflectors are parallel to one another and to the basement surface, whereas some reflectors depart from parallel and show significant topography, consistent with observations of subaerial lava flows, which can display significant roughness (e.g., MacDonald, 1972). Figure 6B, from the lower west flank, exhibits significant variability of intrabasement reflectors in topography, implying complex flow geometries. In some places, the reflectors are horizontal, implying ponded flows. A notable feature of this section of the profile is the existence of segments of steeper intrabasement reflectors. These reflectors could be similar to the foreset beds of Planke et al. (2000) and Spitzer et al. (2008), who suggested that they are caused by volcaniclastics deposited at the toe of a subaerial lava delta.

A depression is observed at the top of the summit at SP 4400 on line A-B (Figs. 1 and 6A). It appears to be a graben and measures ~3 km across and ~55 m in depth (assuming a velocity of 1500 ms^{-1}); it appears to be similar to summit rift zone grabens or calderas on other large volcanoes (e.g., Dieterich, 1988), consistent with the idea that the summit is the volcanic center. A number of secondary cones are observed on line A-B, including a large summit ridge (Toronto Ridge) at SP 5700. These cones have steeper slopes (~5°) than the surrounding volcanic flanks. Large down-to-the-basin normal faults are observed on the western flank at SP 7600 (Fig. 6B) and SP 8400, with ~0.2–0.5 s TWTT of offset (~150–375 m assuming a velocity of 1500 ms^{-1}).

Figure 6. Enlargements of multichannel seismic line A-B and line E-H, illustrating intrabasement reflectors (section A modified from Sager et al., 2013). Uninterpreted data shown in left panel; interpretation is in right panel. Slope indicator refers to the seafloor (vertical exaggeration = 25:1). Dark lines represent intrabasement reflectors. Dashed lines represent faults. Locations are shown in Figures 5 (sections A, B) and 8 (section C).

Other MCS profiles across the axis of the Tamu Massif present characteristics similar to those of line A-B. For example, lines E-F (Fig. 7) and E-H (Fig. 8) also show the rounded, symmetric, shallow slope, across-axis profile of the volcano. In all of these profiles, intrabasement reflectors are observed to dip away from the Tamu Massif summit. The near-summit enlargement of line E-H (Fig. 6C) shows that most intrabasement reflectors dip gently to the basin and are subparallel. The summit reflectors are nearly horizontal and not as continuous as those on the flank, which is similar to the observations on line A-B in Figure 6A. Line E-H also exhibits steeper segments (~3°–5°) of dipping reflectors like those observed on the western flank on line A-B (Fig. 6B), with an appearance similar to sedimentary clinoform layers (e.g., Spitzer et al., 2008). Analogous steeper reflectors are also noted on the other lines that cross the axis of the Tamu Massif (line E-F in Fig. 7).

The depression observed on top of the basement summit on line E-H (Fig. 6C) appears to be a graben. It is ~5 km across and ~170 m in depth (assuming a velocity of 1500 ms^{-1}), similar to that on line A-B (Fig. 6A), implying that this feature is common on the summit of the volcano. The depression on line E-H occurs to the northeast of that on line A-B (Fig. 1), implying that axial rifting follows the southwest-northeast–elongated shape of the Tamu Massif.

Line L-K (Fig. 9) also crosses the axis of the Tamu Massif, but at the northeastern end. Although line L-K shows a rounded profile like line A-B (Fig. 5), it exhibits greater structural complexity. Dips of intrabasement reflectors show at least two major eruptive centers (SP 3900 and SP 4700) and numerous small cones. The implication is that this part of the Tamu Massif had a slightly more complex arrangement of volcanic centers than the center of the edifice. This line crosses Site U1348, which cored a volcaniclastic section, so the cone at SP 4700 is likely made up of volcaniclastics rather than lava flows.

Lines C-I, I-J, J-G, and G-D form a composite profile along the axis of the Tamu Massif (Fig. 10). Although intrabasement reflectors on lines C-I and G-D, at the south and north ends of the massif, respectively, are uniform and descend toward the basin like those noted on across-axis profiles, the basement reflectors on lines I-J and J-G at the summit are subhorizontal and undulatory. In contrast to the across-axis lines, which show a narrow eruptive axis, the along-axis profiles show wide, shallow undulations of intrabasement reflectors, as could be expected from a profile paralleling elongated volcanic centers aligned along the axis. A notable feature of this composite profile is that it shows reflectors clearly to depths of >2 s TWTT. This is equivalent to a depth of ~4 km (assuming a velocity of 4 kms^{-1} for basement), and is below the level of the surrounding abyssal seafloor, implying a remarkable structural consistency of the massif as it formed. In addition, a summit depression, again interpreted as a graben, is seen at the intersections of lines J-G and G-D. It is ~15 km across and ~100 m in depth (assuming a velocity of 1500 ms^{-1}). The location of this graben is the same as that of the graben on line E-H (Fig. 8), implying they are the same feature but in different orientations (Fig. 1).

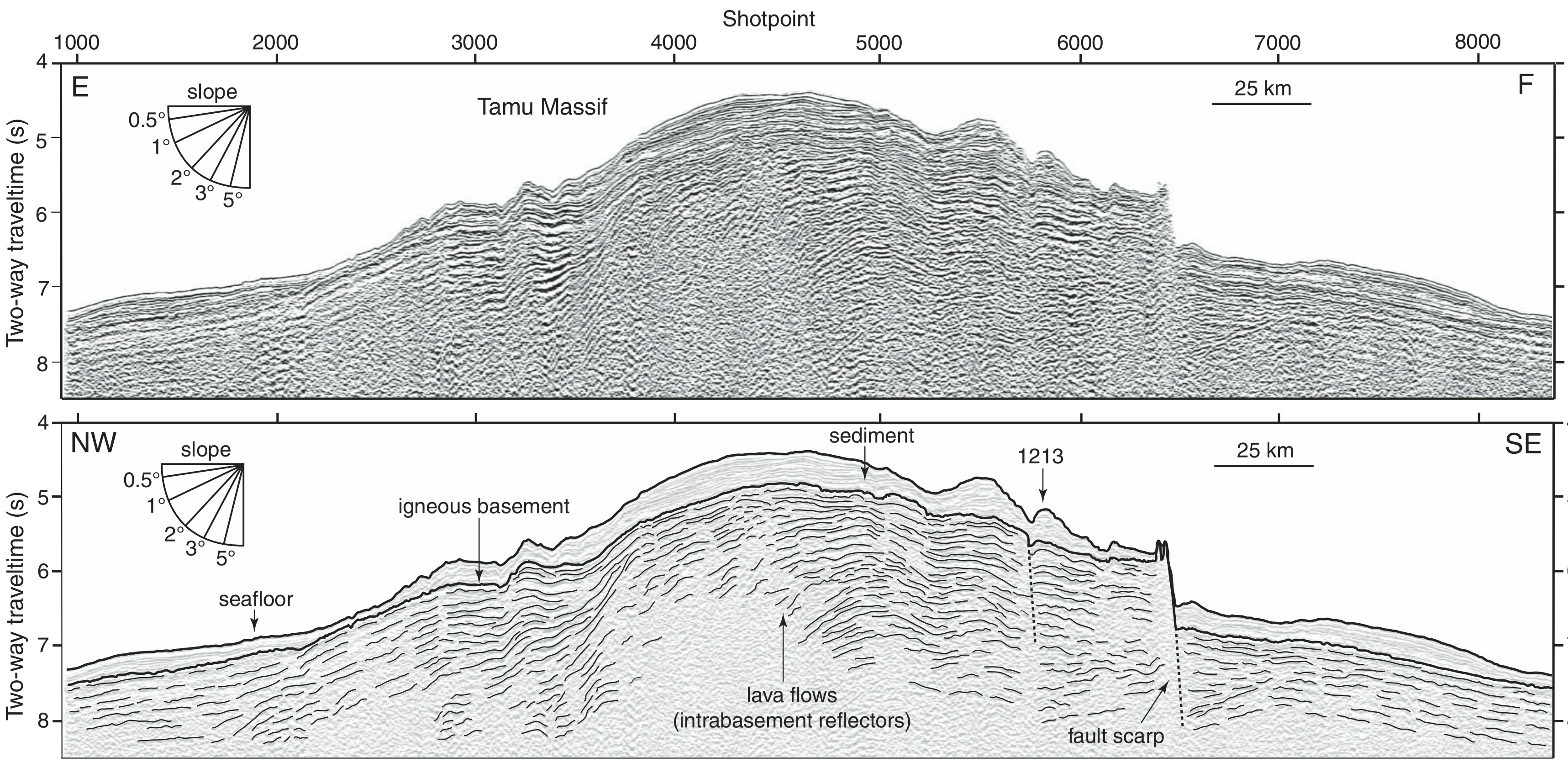

Figure 7. Multichannel seismic reflection profile of line E-F. Vertical exaggeration = 22:1. Other plot conventions as in Figure 5.

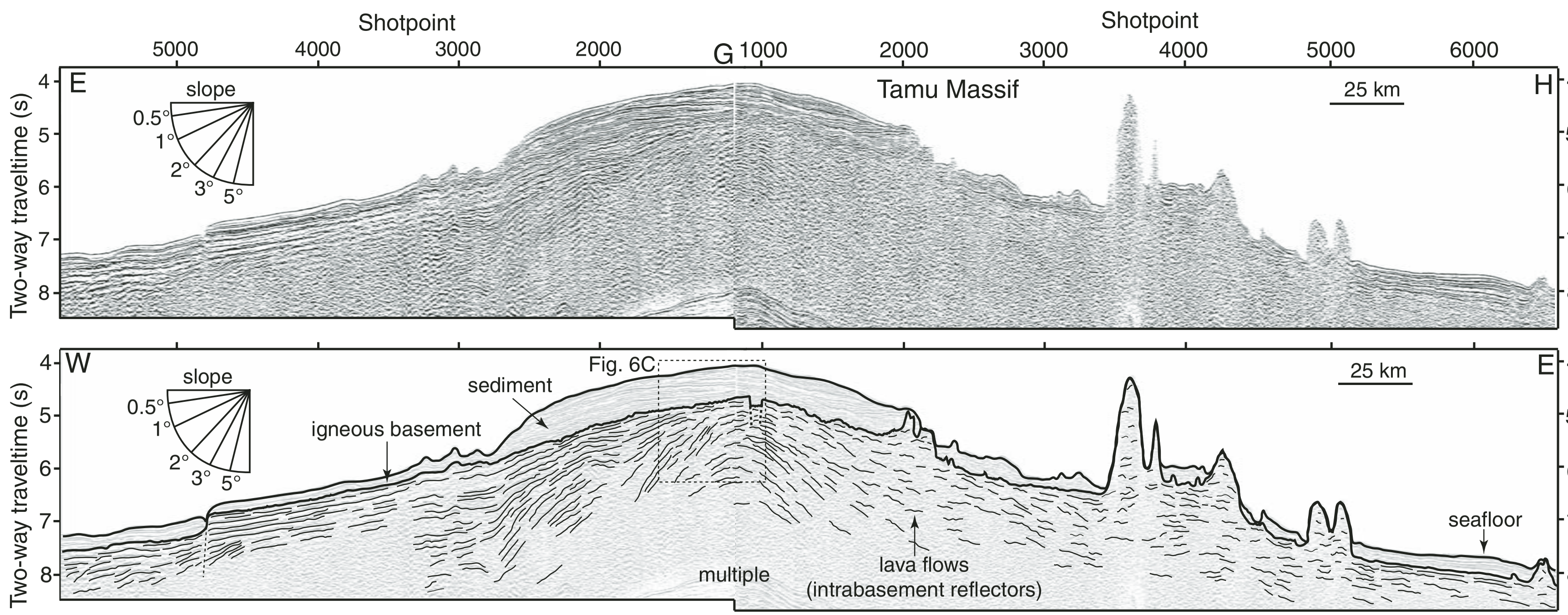

Figure 8. Multichannel seismic reflection profile of line E-H. Vertical exaggeration = 22:1. Boxed area is enlarged in Figure 6. Other plot conventions as in Figure 5.

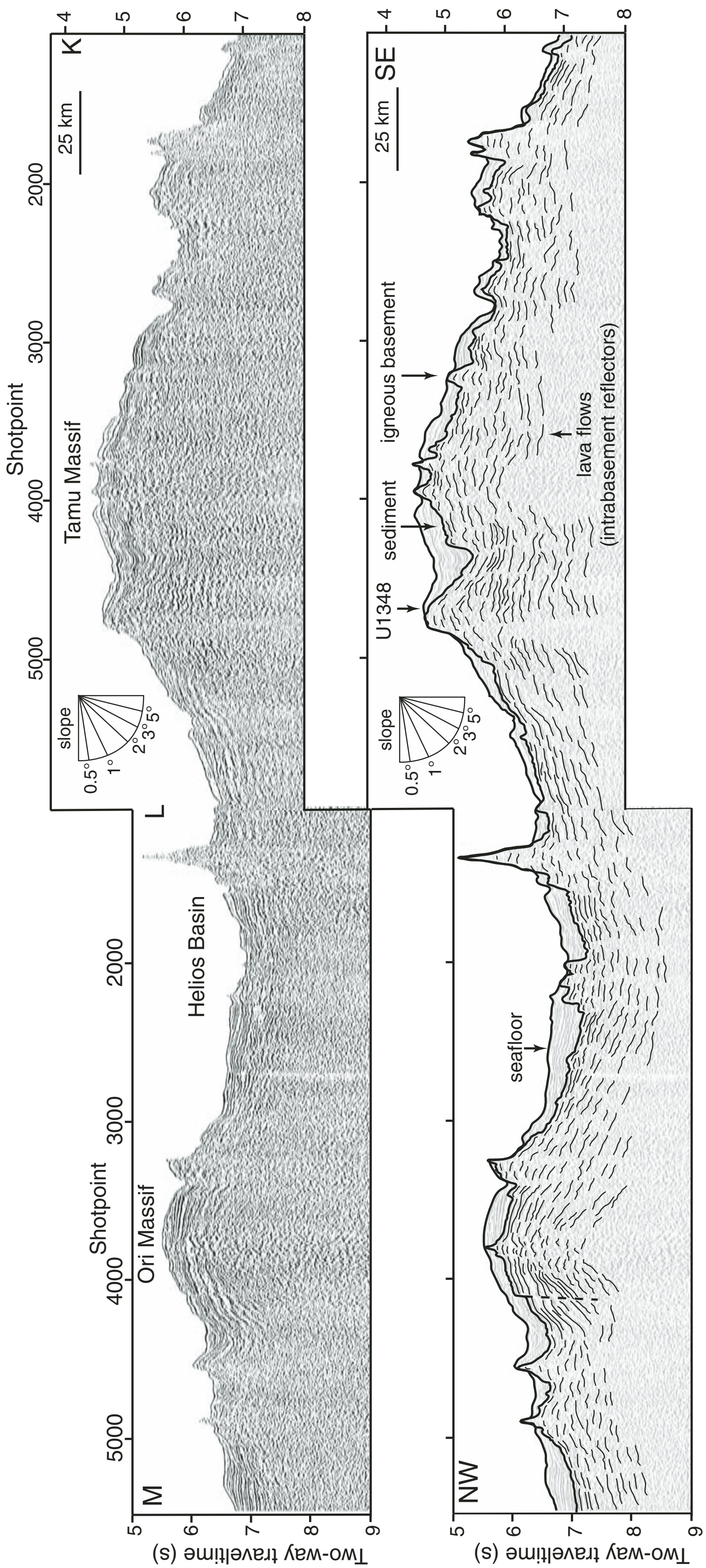

Figure 9. Multichannel seismic reflection profile of line M-K. Vertical exaggeration = 22:1. Other plot conventions as in Figure 5.

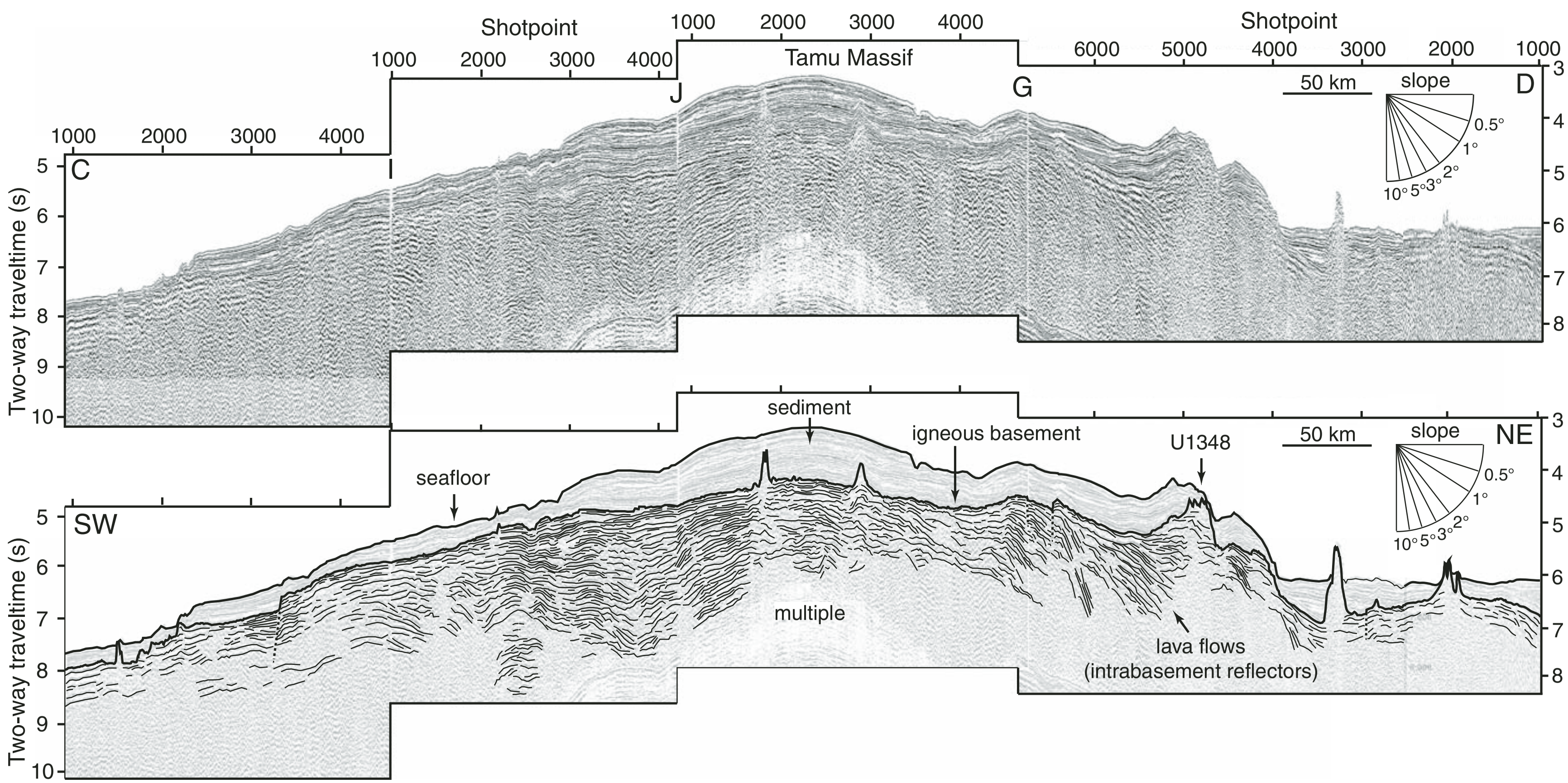

Figure 10. Multichannel seismic reflection profile of line C-D, modified from Sager et al. (2013). Plot conventions as in Figure 5.

For both across-axis and along-axis profiles, secondary cones like those observed on line A-B (Fig. 5) occur on many MCS lines (e.g., line E-H, Fig. 8; line L-K, Fig. 9) and buried cones appear on line J-G (Fig. 10) beneath the thick summit sediment cap. Most are 10–20 km in width and 0.5–1.0 km in height. A few are larger, such as the large ridge on top of the Tamu Massif (Toronto Ridge) (Fig. 5) and the large cone drilled at Site U1348 (Figs. 9 and 10). Some are rounded and some have sharp peaks, and most have flank slopes >5°. Similar features are seen on the TN037 seismic data (Klaus and Sager, 2002) and in bathymetry data. Line C-F (Fig. 11) crosses a low, distal flank salient on the southeast side of the Tamu Massif, and has many small cones of different shapes and sizes. On lines L-K (Fig. 9) and G-D (Fig. 10), Site U1348 is on top of a large basement high that appears to be a volcaniclastic cone, formed by explosive volcanism inferred from volcaniclastic cores recovered at the drill site (Sager et al., 2010).

Similar to the normal faults on line A-B (Fig. 5), large down-to-basin normal faults on the massif flanks are also noted at many locations on the Tamu Massif: lines E-F (Fig. 7), E-H (Fig. 8), and C-I (Fig. 10). The fault at SP 6500 on line E-F (Fig. 7) is especially notable owing to its large throw (~1.0 s TWTT = ~750 m assuming velocity of 1500 ms^{-1}). This fault is also topped by a small volcanic cone, imaged by multibeam bathymetry, where line E-F crosses the fault, suggesting that this fault can be related to secondary volcanism. Although the deeper reflectors on the basinward side of the fault on line E-F bend downward toward the fault, faults elsewhere show simple offset of the basement and intrabasement reflectors on most lines.

Helios Basin

The Helios basin separates the Tamu and Ori massifs and has a rectangular and elongated shape (Fig. 1). It contains several linear seamounts near its center that follow the basin axis (Sager et al., 1999). Magnetic lineations also trend along the basin axis (Fig. 1), so a hypothesis for the basin formation is the splitting of the Tamu and Ori massifs by rifting (Sager et al., 1999; Nakanishi et al., 1999). MCS line M-K (Fig. 9), which crosses the western Helios basin, shows that the volcanic basement of the Tamu and Ori massifs on the basin edges is not cut by large normal faults, as would be expected for a rift basin. Intrabasement reflectors on the Tamu and Ori flanks trend downhill into the basin and meet at the center against the axial volcanic ridge. Line G-D (Fig. 10)

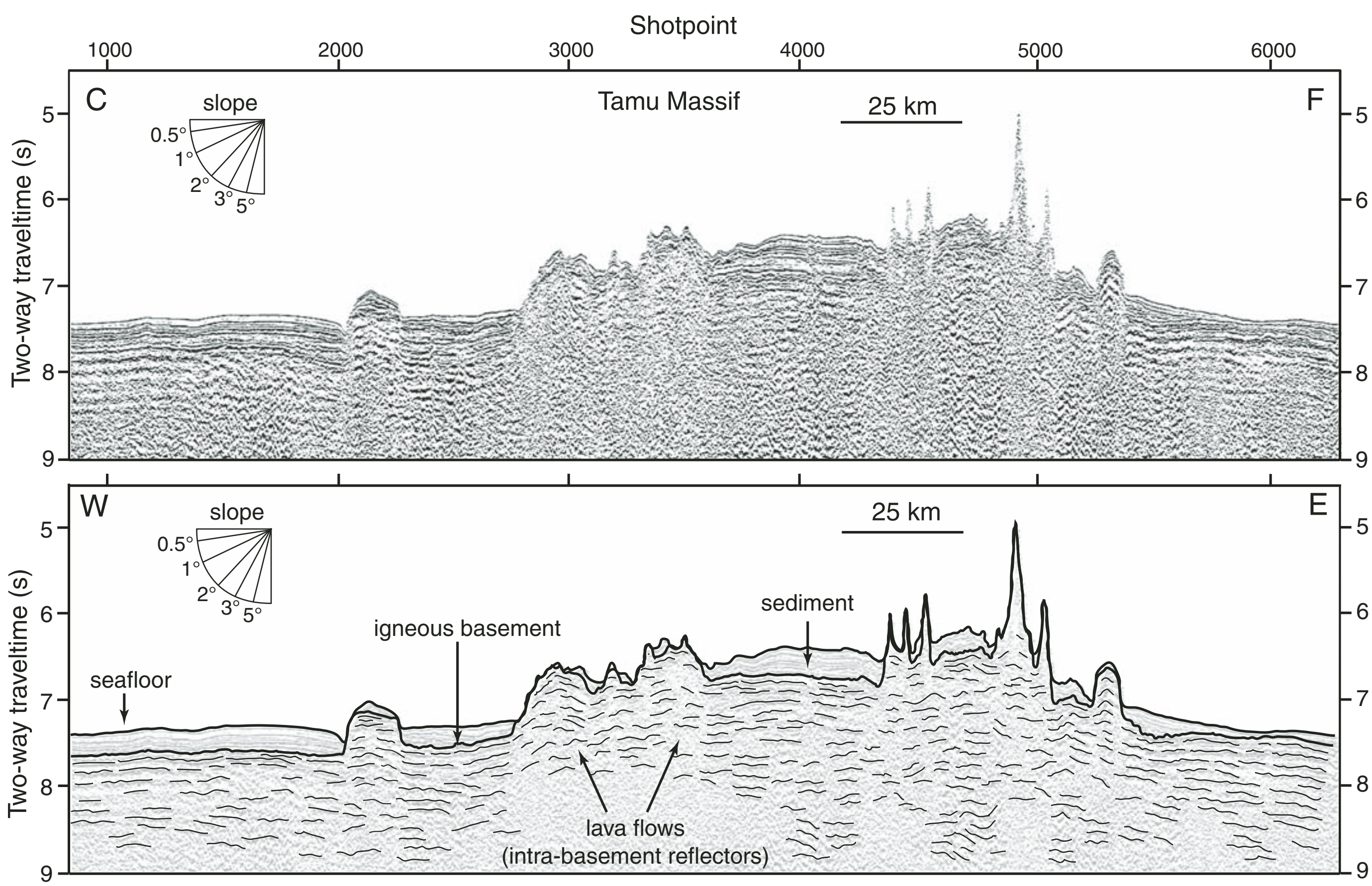

Figure 11. Multichannel seismic reflection profile of line C-F. Vertical exaggeration = 22:1. Other plot conventions as in Figure 5.

crosses the east end of the Helios basin near the northward extension of the Tamu Massif. It also shows descending basement and intrabasement reflectors from adjacent massifs to the bottom of the basin. Few normal faults are seen on this line. A volcanic ridge occurs at the center of a dome-like bulge in the basement surface. Intrabasement reflectors dip outward from the volcanic ridge, implying that it was a volcanic center. Thus, these observations imply that the Helios basin was not formed by the rifting apart of the Tamu and Ori massifs. Instead, the basin apparently formed by seafloor creation during a gap between the construction of the two volcanic centers.

Ori Massif

The Ori Massif is the second-largest and likely second-oldest dome-like volcanic edifice within the Shatsky Rise. MCS line M-D (Fig. 12) crosses this entire edifice in the west-east direction, whereas line M-L (Fig. 9) crosses the west side of the volcano. These profiles provide a structural picture similar to that of the Tamu Massif, showing the Ori Massif to also be a rounded, symmetric volcano with low flank slopes. Intrabasement reflectors mostly dip outward from the summit of the volcano, implying that the Ori Massif is also a large central volcano. In comparison to the Tamu Massif, the Ori Massif has somewhat rougher basement topography. Rough basement shape results from down-to-basin normal faults and secondary cones as well as short-wavelength basement topography. On line M-D (Fig. 12), at the summit of the Ori Massif, the shallowest basement is a ridge (at SP 3700) that was cored at IODP Site U1349 (Sager et al., 2010). In addition, line M-L (Fig. 9) shows similar features including rough basement caused by secondary cones and down-to-basin faults. A volcanic center is imaged at SP 3800 (Fig. 9); it displays a pattern of intrabasement reflectors dipping outward from the center. The center of the pattern is approximately beneath the highest point of the basement surface, implying that the volcanic center did not move laterally as it built. Moreover, the basement summit on this line is topped by a small volcanic cone, which is likely a late-stage eruption product.

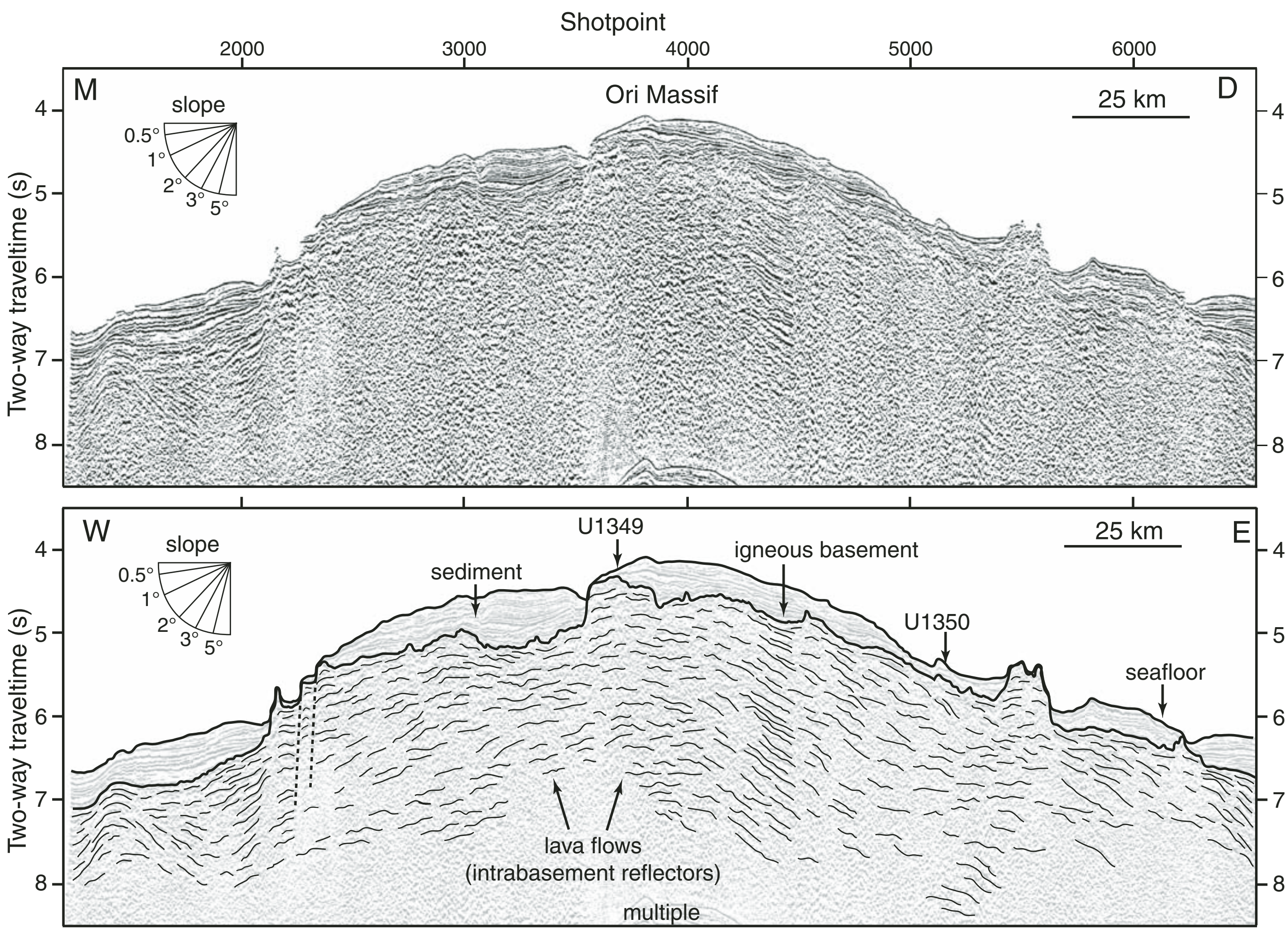

Figure 12. Multichannel seismic reflection profile of line M-D. Vertical exaggeration = 22:1. Other plot conventions as in Figure 5.

Massif Summit Basement Morphology

Although the seismic lines are sparse, limiting the resolution of summit basement features and possibly missing small features, the data nonetheless reveal the broad-scale summit structure of the three massifs (Fig. 13). The Tamu Massif summit has two large basement peaks that imply two volcanic centers. As stated herein, the eastern peak is rounded and has low slopes and appears to be the center of the volcano shield-building stage. The Toronto Ridge, on the west side of the summit, is tall (~1 km height), linear, and has steeper slopes than the shield stage (~5° compared to <1°). The Tamu Massif summit map also shows several small buried cones. These are likely secondary cones such as those that dot the volcano flanks. Moreover, although line A-B could be interpreted to show a basin between the two Tamu basement peaks, the Tamu Massif summit map shows that there is no closed basin. A remarkable feature of the Tamu Massif summit is that despite the fact that shallow-water sediments have been recovered around the summit (Sager et al., 1999, 2010), no evidence of erosional truncation or flattening is observed around the summit in seismic sections.

The Ori Massif summit has two large basement peaks. One basement peak occurs at the center and corresponds to the summit ridge (<0.5 km height) seen on line M-D at SP 3700 (Fig. 12). This peak has a nearly flat top and contains nearly horizontal intrabasement reflectors. Cruise TN037 seismic data show that the other large basement peak on the northeast side of the Ori summit is a rounded ridge (~1 km height and ~5° slope) (Sager et al., 1999), similar to the Toronto Ridge on the Tamu Massif. As with the Tamu Massif, cores from Site U1349 at the Ori Massif summit indicate shallow water, but seismic sections show no unequivocal evidence of erosion or truncation.

The Shirshov Massif summit shows one larger basement peak on the west side of the summit platform and three smaller cones on the east side of the summit. Cruise TN037 seismic data show that the large basement peak has an overall rounded shape with two small secondary cones on top (Sager et al., 1999). The buried cones on the east side appear similar to other secondary cones on the Tamu and Ori massifs. Although much of the Shirshov Massif summit basement surface appears flat (Sager et al., 1999), detailed examination shows that the basement surface is undulating and shows no evidence of truncation. Thus, it does not appear to be an erosional feature. Furthermore, the summit cones are apparently constructional features, not erosional remnants. Therefore, like the Tamu and Ori massifs, the summit of the Shirshov Massif does not appear eroded and summit cones appear to be secondary features.

DISCUSSION

Geologic Interpretation of Intrabasement Reflectors

Based on the synthetic seismograms, reflections occur where large-scale changes in density and sonic velocity occur.

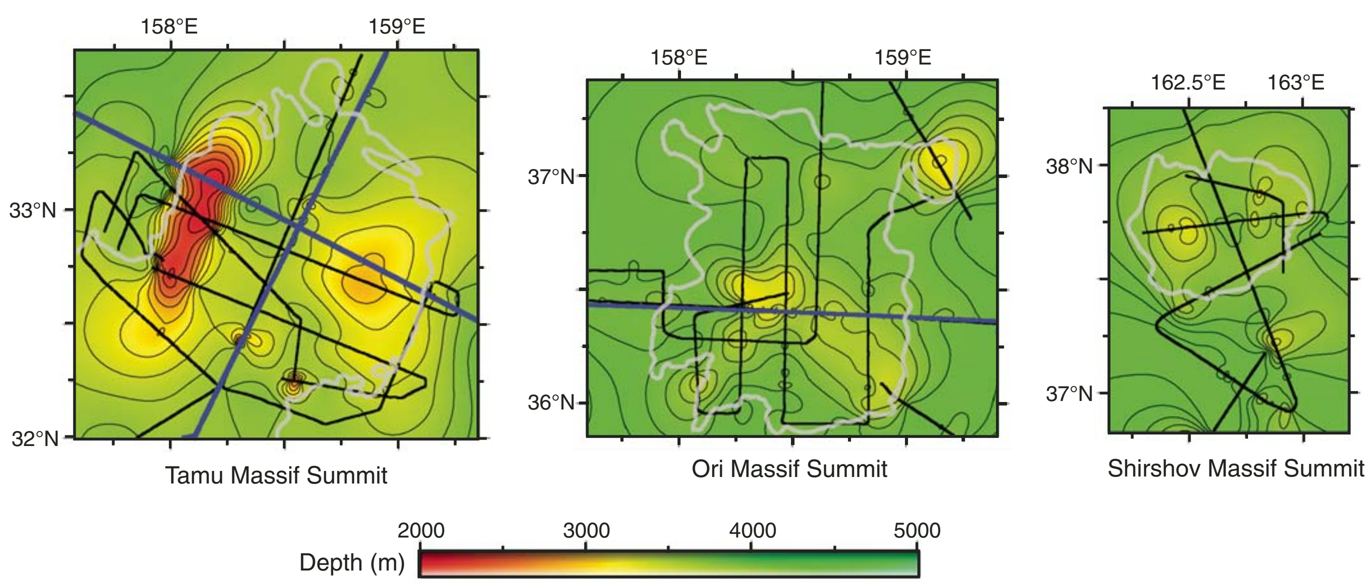

Figure 13. Summit basement morphology maps. Isobaths are gridded from the combined seismic data set of R/V *Marcus G. Langseth* multichannel seismic data and seismic data from cruise TN037 (Klaus and Sager, 2002). The average velocity of the sediments and water column were assumed to be 2000 ms^{-1} and 1500 ms^{-1}, respectively. Basement contours are shown at 200 m intervals. Locations and extents of these maps are shown in Figure 1. Heavy blue and black lines show the seismic lines used to determine basement depths (dark blue—R/V *Marcus G. Langseth*; black—cruise TN037). Heavy gray contours show the 3000 m depth contour (left) and 3500 m depth contour (middle, right) from satellite-derived bathymetry data (Smith and Sandwell, 1997) for positional reference.

In our sections, these are usually changes in lithology, including the sediment-igneous basement interface, alternations of packages of pillow flows and massive flows, and thick interflow sediment layers. A high-amplitude basement reflection occurs at the top of the igneous crust, resulting from the large increase in density and sonic velocity at that interface. In most places it can be recognized because of its amplitude, the contrast of its rugged surface with smoother sediments above, and the fact that it is an angular unconformity in many spots. In some places, however, intrabasement reflectors are subparallel to sedimentary reflectors and the basement acoustic contrast is not strong, so the igneous basement interface can be difficult to recognize. Nevertheless, in such places it is usually possible to follow the igneous basement surface from adjacent regions where it is clear.

Within the igneous basement, given the long wavelength of the sound source and the synthetic seismogram results, individual lava flows are not usually resolved because they are frequently too thin to cause an individual reflection or there is no significant velocity-density contrast across the flow boundaries. Instead, intrabasement reflectors are typically the surfaces of packages of lava flows where gross changes in lithology occur. For example, this occurs as at Site U1347 where a zone of pillow lavas punctuates a series of massive flows (Fig. 3), resulting in a decrease in sonic velocity and density between the dense massive flows. This change in properties probably occurs because the pillows are frequently separated by rubble and volcaniclastic sediment, which has lower bulk density and velocity compared to the massive flows. This finding is similar to interpretations of seismic data from the Ontong Java Plateau, in which intrabasement reflections are thought to result from alternating groups of pillow and massive lava flows (Inoue et al., 2008). At Site U1347, we also observe reflectors apparently caused by the contrast between massive flows and thick interflow sediment layers (Fig. 3). Site U1348 is a different situation because only volcaniclastic material was recovered and this lithology has many short-wavelength reflectors (Fig. 3). This signature is apparently a result of highly variable density and sonic velocity caused by layering within the volcaniclastics. Although the intrabasement reflections usually occur from alternations of lithology, these changes occur at lava flow surfaces, so the seismic images are nevertheless useful to illustrate the structure of lava flows. Similar interpretations have been made for intrabasement reflectors within other oceanic plateaus (Rotstein et al., 1992; Uenzelmann-Neben et al., 1999; Inoue et al., 2008).

The correlation between the seismic reflections and the geology from synthetic seismograms gives us a key for interpreting igneous basement reflection patterns. Seismic layering results from the transition between sediments and igneous rocks, the surfaces of lava flow packages, and gross changes in lithology that are usually bounded by lava flows. Thus, the basement reflector shape illustrates the morphology of the igneous basement surface and the intrabasement reflector geometries mainly denote sequences of lava flows.

Structure and Evolution of the Shatsky Rise Massifs

The basement reflectors show that the igneous basement surface for both the Tamu and Ori massifs is relatively smooth, with a shallow slope, and is punctuated with secondary cones. Typical slopes are ~1°–1.5° on the upper flanks and <0.5° on the lower flanks. Analogous shallow slope characteristics are observed in Iceland, which is a large volcanic edifice formed at the Mid-Atlantic Ridge (Tryggvason and Bath, 1961; Rutten, 1964; Rossi, 1996; Sager et al., 1999). Considering the similar divergent plate boundary settings for both the Shatsky Rise and Iceland, shallow slope angles may be a result of large volcanic eruptions on the thin and weak lithosphere at mid-ocean ridges. Moreover, high-effusion-rate eruptions (indicated by the massive lava flows of the Tamu Massif) may result in large areas covered by shallow-angle lava flows (Sager et al., 2010; Bryan et al., 2010). Given that the slopes of the Ori Massif are similar to those of the Tamu Massif, whereas no thick, massive flows were cored from the Ori Massif (Sager et al., 2010), the tectonic setting may be the primary factor controlling the slope.

Intrabasement reflectors are continuous over lengths of several to tens of kilometers (Figs. 6A and 6B), but piecewise-continuous over hundreds of kilometers (e.g., Fig. 5). They are not as clear, conformable, and continuous as typical sedimentary reflectors, but this is not a surprise because lava flows have rougher surfaces. Overall, the reflectors show a pattern of gently dipping lava flow packages trending downhill from the volcanic centers.

The basement and intrabasement reflectors show that the Tamu Massif is a large central volcano. Lava flows dip away from the summit in all directions on all MCS lines that cross the massif. Those profiles that cross the southwest-northeast–trending axis of the Tamu Massif (e.g., Figs. 5, 7, and 8) show a rounded summit and lava flows inclined down the shallow slope. The composite profile that extends along the axis of the Tamu Massif (Fig. 10) shows even shallower slopes, but flows also trend downward from the summit. Although many secondary cones are observed, no significantly large sources of lava flows exist except the summit. An important implication is that the source of lava flows is at the center of the Tamu Massif. This is different from continental flood basalts, which are thought to be constructed by fissure eruptions from multiple locations (Jerram and Widdowson, 2005; Bryan et al., 2010). Our data do not rule out fissure eruptions as a source because individual eruptions cannot be distinguished; however, the data are clear that the pattern of lava flows dipping away from the summit is consistent. This pattern is different from Iceland (Sigmundsson, 2005) and possibly other large oceanic plateaus (e.g., Kerguelen Plateau, Rotstein et al., 1992; Ontong Java Plateau, Inoue et al., 2008), which may have formed as composite features from multiple volcanic sources. The reason the Tamu Massif formed as a single volcano may be that the Pacific plate drifted rapidly relative to the volcanic source, so that subsequent large eruptions did not overlap (Sager et al., 2013).

The Ori Massif also appears to be a large central volcano with structure similar to that of the Tamu Massif, but smaller in size. Although we have only two MCS lines that cross it, which means that important details may be missed, it appears to be a broad, central volcano. There were no thick massive flows recovered from the Ori Massif (Sager et al., 2010), but it is also an immense volcano; therefore, thick, massive flows may not be required to build a large volcano, but rather thinner flows could also do so. Thick massive flows may be required to form volcanoes the size of the Tamu Massif.

Basement and intrabasement reflectors on the lower flanks of the Tamu and Ori massifs are smooth in all directions, indicating that the massifs are not fault bounded. On line A-B, which crosses the Tamu Massif along its shortest dimension, the volcano is >550 km in width (Fig. 5). This line appears to be the only seismic line that extends beyond the plateau into the adjacent basin; on most other profiles, igneous basement is still deepening at the profile limits. On the west side of this line, the Tamu Massif basement declines at shallow angles and merges smoothly with that of the surrounding ocean crust, so that it is impossible to tell precisely where the lower flank of the Tamu Massif ends. This observation suggests that long flows covered a wide area around the plateau and that estimates of the Shatsky Rise area and volume, which defined the limit by a lower flank depth contour (Sager et al., 1999), are underestimated. The lack of a sharp boundary also indicates that the plateau is not fault bounded, as was inferred from the proximity of plateau formation to the triple junction and the alignment of plateau edges with magnetic lineations (Sager et al., 1999). This is also true for the north flank of the Tamu Massif and south flank of the Ori Massif (bordering the Helios basin), where it was proposed that rifting occurred related to seafloor spreading (Sager et al., 1999). The absence of obvious faults caused by rifting in the MCS data implies that this interpretation is incorrect.

In MCS profiles crossing both the Tamu and Ori massifs, intrabasement reflectors are seen to depths of 0.5–2.5 s TWTT beneath the basement surface (Figs. 10 and 12). At a velocity of 4 kms^{-1}, which is typical for the upper igneous crust (Korenaga and Sager, 2012), this time corresponds to 1–5 km depth. Because the massifs are ~3 km in height, this means that some of these reflectors are near or below the regional abyssal plain depth. In general, intrabasement reflectors display a shape parallel to the basement surface at depth, implying stability of the volcanic structure. Beneath the summits of both the Tamu and Ori massifs, intrabasement reflectors show that the summit shape remains the same for several kilometers depth. This observation implies long-term stability of the summit location. Furthermore, the consistent flank shapes of both edifices imply an emplacement process that maintained isostatic balance. Had volcanism been concentrated solely at the summit of the volcano, the weight of the new lava flows would have depressed the center and buried lava flows would dip toward the center, as is observed for seaward-dipping reflector sequences on continental margins (Mutter, 1985; Planke and Eldholm, 1994; Planke et al., 2000). The fact that the Shatsky Rise lava flows are parallel to one another and to the basement surface indicates that the lavas are not concentrated at the summit, but spread over the entire surface, so no one part is pushed down relative to others. Furthermore, the emplacement of mass must be balanced to maintain the shape of these volcanoes. This result likely occurs from emplacement of material to the volcano root that balances the material added on top: otherwise the geometry would change with time as material at the top is added. The Shatsky Rise was formed at a triple junction and the lithosphere near oceanic ridges is thin and weak, implying no lithospheric strength (Sager et al., 1999; Nakanishi et al., 1999), so the Shatsky Rise volcanoes may be in isostatic balance at all times.

The MCS profiles exhibit steeper segments (~3°–5°) of dipping reflectors in some places (e.g., Figs. 5 and 8) compared to the shallow flank slopes (<0.5°–1.5°) of the volcanoes. The cause of these steeper sections is uncertain, but a possibility is that lava deltas build outward like sedimentary deltas, with steeper slopes on the leading edge. Planke et al. (2000) and Spitzer et al. (2008) attributed steeper foreset beds in seaward-dipping reflector sequences as indicators of volcaniclastic debris formed near sea level at the toe of advancing lava flows. It is unclear whether the steeper dip of intrabasement reflectors on the Shatsky Rise MCS profiles has the same connection to sea level. In many places where they are observed (e.g., Fig. 6), these reflectors are too deep to have reached their present depths through normal subsidence (see subsidence curves in Sager et al., 2010), implying another cause.

Large down-to-basin normal faults on massif flanks are observed at many locations (Fig. 1). They show offset of the basement and intrabasement reflectors (0.1–1.0s TWTT = ~75–750 m at a velocity of 1500 ms^{-1}). A possible explanation for these faults is rifting related to seafloor spreading around Shatsky Rise. The distribution and orientation (observed in multibeam bathymetry data) of faults show no apparent correlation to nearby magnetic lineations. Moreover, it seems unlikely that seafloor spreading–related rifting would produce consistently asymmetric faulting. All of the major faults have a down-to-basin geometry. Another possible explanation for these faults is differential subsidence, the volcano center subsiding less than the flanks because of magmatic underplating beneath the volcanic center (e.g., Ito and Clift, 1998). This suggestion implies that down-to-basin faults should be found on all sides of the Shatsky Rise; however, the large down-to-basin normal faults are observed only on the western flanks of the rise (Fig. 1). Although existing data are sparse and probably do not show all such faults, the uneven distribution of normal faults is an unexplained complexity to the Shatsky Rise subsidence history.

Secondary cones are seen on almost all seismic lines and it appears that they are scattered across the volcano at all depths, with no particular area of concentration. Their seemingly random distribution suggests that they are not tied to any large-scale structure. Given that ~36 such cones are observed on the Tamu Massif seismic lines (Figs. 5, 7–11), which sample only a small area (<5% of the entire Tamu Massif), there must be hundreds of secondary cones that dot the flanks of this volcano. The secondary cones range from small (<5 km wide, a few hundred meters height) to large (tens of kilometers across and ~1 km in height) (e.g., Figs. 5 and 9). Generally they have steeper slopes (~5°) and are sometimes conical but sometimes complex in topographic structure (e.g., Fig. 11). Bathymetric maps derived from satellite gravity image them poorly, but many have been observed in shipboard bathymetry data. In many large volcanoes (e.g., Hawaii; Macdonald and Abbott, 1970), secondary cones occur along rift zones because these are the sources of major eruptions, but that does not appear to be true for Shatsky Rise. Perhaps these secondary cones are formed when lava flows are constrained from lateral flow and break out vertically. The large basement high on which Site U1348 was drilled appears to be a significant secondary source of volcanism. It is an approximately cone-shaped feature ~25 km across and ~1 km in height (Figs. 9 and 10). Volcaniclastics were cored at its summit, implying explosive shallow-water volcanism (Sager et al., 2011). Its summit was also near sea level, as shown by shallow-water fossils (Sager et al., 2010). Although the Site U1348 cores imply that many secondary cones consist of volcaniclastic material, some are basaltic cones, such as those that form on other large volcanoes (Beiersdorf et al., 1995). Basalt rocks were dredged from Toronto Ridge and summit ridges on Ori Massif (Sager et al., 1999).

Summit Morphology and Sea Level

Summit basement morphology maps show that large basement peaks are common on top of the large Shatsky Rise massif volcanoes. The Tamu Massif has two large basement peaks, the eastern broad rounded peak and the Toronto Ridge (Fig. 5). The broad rounded peak has low slopes and is the center of the volcano shield-building stage. The Toronto Ridge has a rounded top, although there is a break in slope between the top and the steeper flanks. Its depth (~2 km) would have made it subaerial when the deeper summit was erupted, as inferred from shallow-water sediments recovered at nearby Site U1347 (Sager et al., 2010), which is ~2 s TWTT (~1.5 km) deeper. The lack of evident erosion due to subaerial exposure implies that this ridge is a late-stage volcanic eruption, emplaced after significant subsidence of the volcano. Furthermore, its steeper side slopes imply a different style of volcanism from the Tamu Massif shield-building stage, similar to that of the secondary cones on the massif flanks or normal seamounts.

The Ori Massif summit also shows two large basement peaks. One, on the northeast side of the massif summit, has a rounded top, similar to the Toronto Ridge on the Tamu Massif (Sager et al., 1999). The other, at the central summit, has a nearly flat top and intrabasement reflectors that are nearly horizontal (Fig. 12). The Shirshov Massif summit has one large basement peak with a rounded shape similar to other secondary cones (Sager et al., 1999). Layering within this peak follows its slopes, implying that it is a volcanic cone rather than an erosional remnant.

Although the large basement peaks at the three massif summits have different structures, we see similar features on other seismic lines at different locations. On line C-F (Fig. 11), which crosses a low ridge on the south distal flank of the Tamu Massif, there are examples of three different cone structures. Between SP 4900 and SP 5100, there are two secondary cones that display sharp peaks (the sharpness is a result of the vertical exaggeration; the true slopes are only ~5°–10°). Such cones are typical of the secondary cones that dot the Shatsky Rise flanks. At SP 5400, a broader cone occurs with a rounded top. Within this cone, seismic layering is observed to follow the summit shape (i.e., bowed upward). This cone is similar to the Toronto Ridge on the Tamu Massif and the ridge on the northeast side of the Ori Massif summit. At SP 2100, a flat-topped ridge is observed, similar to the central Ori Massif summit ridge. Its steep sides and the apparent truncation of internal parallel reflectors along the sides could indicate bounding normal faults as well. However, interpreting both of these similar features as horst blocks makes little sense, because there is no obvious mechanism to down-fault the volcano surrounding each of these cones. Furthermore, because of the depth of the cone on line C-F, the flat summit cannot be attributed to erosion at sea level. Instead, we think that the flat interior structure and top are constructional features. Consequently, all of the summit ridges on the three massifs imply that volcanism continues and changes character after the initial shield-building stage of massive volcano construction. Similar features on other large volcanoes form long after the main shield-building volcanism has concluded (Macdonald and Abbott, 1970) and circumstantial evidence from the Shatsky Rise volcanoes implies the same.

According to the evidence from samples recovered by drilling and dredging, the summits of the three massifs within the Shatsky Rise must have been in shallow water when volcanism ceased. Shallow-water fossils were dredged from a secondary cone at ~3000 m depth on southeast side of Tamu summit (Sager et al., 1999). Moreover, evidence for shallow water was found in basal sediments for Sites U1347, U1348 (Tamu Massif upper flanks), U1349 (Ori Massif summit), and U1346 (Shirshov Massif summit) (Fig. 1). These findings agree with backtracking of the sites using subsidence models, which also imply the sites would have been in shallow water when the sediments were deposited (Sager et al., 2010). Given that Site U1347 is ~800 m deeper than the shield summit of the Tamu Massif, it was inferred (Sager et al., 2010) that the summit may have been subaerial. This inference seems contradicted by the lack of obvious subaerial erosion on seismic lines. Line A-B (Fig. 5) is the only MCS line over the shallowest part of the summit. It shows no notching or flattening of the summit owing to erosion. Cruise TN037 seismic lines also cross the Tamu Massif summit and show no evidence of erosion (Sager et al., 1999; Klaus and Sager, 2002). Because all of the evidence on the Tamu Massif for sea level is from sediments interpreted as deposited in shallow water (not actual evidence of exposure), we infer that the Tamu Massif reached near sea level, but was not emergent. The Ori Massif is similar because seismic lines over this volcano also show no evidence of significant subaerial erosion (Figs. 9 and 12). The only evidence of emergence is from the top of the summit ridge, where the juxtaposition of a paleosol and shallow-water carbonate sediment layer imply formation exactly at sea level (Site U1349; Fig. 1) (Sager et al., 2010). This ridge was likely the highest point on the Ori Massif, suggesting that the bulk of the volcano formed below sea level. Site U1346, at the north edge of the Shirshov Massif summit (Fig. 1), indicates a shallow-water depositional environment (Sager et al., 2010), and the Shirshov Massif summit has an overall flat basement structure that has been interpreted as a subaerially eroded summit platform (Sager et al., 1999); however, the TN037 seismic data show no evidence of erosion on the Shirshov Massif summit (Sager et al., 1999; Klaus and Sager, 2002). The summit cones are not erosional remnants and the summit platform is undulatory and shows no truncation of basement layering; therefore, the Shirshov Massif may have stayed submerged.

Calderas are common features at the summits of large volcanoes and result from collapse of evacuated magma chambers near the end of the volcano history (MacDonald, 1972). Usually, these features exist near or at the eruptive sources. Two summit grabens are observed on the Tamu Massif (Figs. 5, 6, 8, and 10) that range from ~55 to 170 m in depth and ~3 to 15 km across. Both dimensions and locations where the depressions are found are similar to those of calderas on other large volcanoes (MacDonald, 1972; Walker, 2000), suggesting that they may have an analogous origin (Sager et al., 2013). The two observed depressions are ~100 km apart (Fig. 1), but occur along the southwest-northeast axis of the elongated shape of the Tamu Massif. Because there are no intervening seismic lines, it is impossible to tell whether they are connected. Both occur along the Tamu Massif summit, consistent with the idea that the Tamu Massif formed mainly from summit eruptions (Sager et al., 2013). No similar collapse depressions are found on the Ori and Shirshov massifs, but data are sparse and collapse depressions may have been undetected by existing tracks.

Origin of the Shatsky Rise

Near-surface structure is not diagnostic of the proposed mechanisms (plume or non-plume) of oceanic plateau formation, so surface geophysical data are not suited to determine unequivocally which mechanism is correct. However, some of the observations made here can help constrain the explanations used for oceanic plateau formation. Combined with drilling data (Fig. 2; Sager et al., 2013), the seismic data offer a compelling view of the Shatsky Rise as consisting of several immense volcanoes. The Tamu Massif is the largest and oldest volcano within the Shatsky Rise, and it appears to be a single volcano the size of the largest volcanoes in the solar system, and possibly the largest single volcano on Earth (Sager et al., 2013). Such a large volcano, characterized by massive lava flows, implies massive and rapid eruptions. Therefore, whatever mechanism is used to explain the formation of the Shatsky Rise, it must be able to emplace an immense amount of magma, forming a large volcano at one place and perhaps in a short time. This result probably fits with the plume head hypothesis, as does the evident trend to smaller volcanic output with time, i.e., the Ori and Shirshov massifs (Sager, 2005). However, the large size of volcanic constructs is not necessarily diagnostic of the plume model, because decompression melting at plate boundaries (the plate model) also could form large volcanic edifices (Foulger, 2007). It is clear from magnetic lineations that the Shatsky Rise formed at a ridge-ridge-ridge triple junction (Nakanishi et al., 1999), so the plateau is definitely linked to plate boundary mechanism. Unfortunately, little evidence found from the MCS data supports the idea of spreading-ridge rifting on the flanks of the Shatsky Rise massifs. If the Shatsky Rise formed from rifting-related decompression, it must have concealed the evidence of rifting.

Although the Shatsky Rise is composed of several enormous volcanoes, it appears to have remained mostly submerged, because seismic data show no evidence of the subaerial erosion that would be caused by significant uplift. This observation does not appear to fit the simple thermal plume head hypothesis, which calls for significant dynamic uplift (e.g., Coffin and Eldholm, 1994). However, it is notable that the larger Ontong Java Plateau also stayed submerged during its formation (Fitton et al., 2004). One explanation for submarine eruptions of Ontong Java Plateau is that dense fertile mantle was entrained by rapid seafloor spreading and this dense mantle material caused the plateau to be isostatically depressed and to subside anomalously (Korenaga, 2005). The Shatsky Rise also formed near fast spreading ridges (Nakanishi et al., 1999), and its crustal velocity structure suggests that the mantle source was chemically anomalous (Korenaga and Sager, 2012), so it may have undergone similar mantle dynamics. This similarity suggests that some factor in the formation of some basaltic oceanic plateaus keeps them from rising above the sea surface.

CONCLUSIONS

Modeling and correlation of synthetic seismograms using core and log velocity and density data from scientific drilling sites crossed by MCS lines establishes the seismic response to geology for the Shatsky Rise volcanoes. High-amplitude basement reflections result from the transition between the sediment and igneous rock. Intrabasement reflections are caused by alternations of lava flow packages with differing properties and by thicker interflow sediment or volcaniclastic layers. Therefore, the basement and intrabasement reflectors can be traced in the MCS profiles to examine the morphology of the igneous basement surface and the structure of lava flows below that surface.

The overall structure of the Shatsky Rise shows that the plateau is composed of several immense central volcanoes. The Tamu Massif, the largest and oldest volcanic edifice within the Shatsky Rise, is a massive dome-like volcano. It is characterized by shallow flank slopes (<0.5°–1.5°) constructed by lava flows mostly emanating from the volcano center and extending hundreds of kilometers down the generally smooth flanks to the surrounding seafloor. The morphology of the massif implies formation by extensive and far-ranging lava flows emplaced at small slope angles. The relatively smooth flanks indicate that no significant rifting occurred due to spreading ridge tectonics, even though the Shatsky Rise formed at a triple junction. In addition, the shape of the volcanic center appears to remain stable because the underlying lava flows follow the same shape at depth, suggesting that the volcanic emplacement must be in isostatic balance at all times. Important implications are that the addition of material cannot be concentrated at the center of the volcano, or it would subside more than the flanks, and that isostatic balance requires the addition of material to the volcano root to balance eruptions on the surface. The Ori Massif is another large central volcano with similar structure, but smaller in size compared to the Tamu Massif. The Ori Massif also shows no evidence of spreading ridge rifting on its flanks. The basin between the Tamu and Ori massifs (Helios basin), which was thought to have formed by rifting, is not bounded by large faults, and instead reflects a gap in the volcanism between the two volcanoes. Shallow-water evidence was found from drilling and dredging either at the summits or on the upper flanks of all three massifs of Shatsky Rise, suggesting that the summits of the massifs must have been in shallow water when they formed. In contrast, the seismic data show no evidence of subaerial erosion, implying that these volcanoes were never highly emergent.

ACKNOWLEDGMENTS

We thank the Captain, crew, and technical staff of the R/V *Marcus G. Langseth* for assisting in collection of geophysical data during two cruises. We are indebted to Seismic Micro Technology, Inc., and Halliburton, Inc. for making seismic analysis software available at no cost or reduced cost. We thank Sean Gulick and an anonymous reviewer for helpful critiques. This project was funded by National Science Foundation grants OCE-0926945 and OCE-0926611, National Natural Science Foundation of China grants 91328205 and 41376062, Key Laboratory of Marine Mineral Resources, Ministry of Land and Resources grant KLMMR-2014-B-06, the China Scholarship Council for Joint Education Program between Texas A&M University, and the Ocean University of China.

REFERENCES CITED

Anderson, D.L., Tanimoto, T., and Zhang, Y.S., 1992, Plate tectonics and hotspots: Third dimension: Science, v. 256, p. 1645–1651, doi:10.1126/science.256.5064.1645.

Ballard, R.D., Holcomb, R.T., and van Andel, T.H., 1979, The Galapagos Rift at 86°W: 3. Sheet flows, collapse pits, and lava lakes of the rift valley: Journal of Geophysical Research, v. 84, p. 5407–5422, doi:10.1029/JB084iB10p05407.

Beiersdorf, H., Bach, W., Duncan, R., Erzinger, J., and Weiss, W., 1995, New evidence for the production of EM-type ocean island basalts and large volumes of volcaniclastics during the early history of the Manihiki Plateau: Marine Geology, v. 122, p. 181–205, doi:10.1016/0025-3227(94)00107-V.

Bercovici, D., and Mahoney, J., 1994, Double flood basalts and plume head separation at the 660-kilometer discontinuity: Science, v. 266, p. 1367–1369, doi:10.1126/science.266.5189.1367.

Bryan, S.E., Peate, I.U., Peate, D.W., Self, S., Jerram, D., Mawby, M.R., Marsh, J.S., and Miller, J.A., 2010, The largest volcanic eruptions on Earth: Earth-Science Reviews, v. 102, p. 207–229, doi:10.1016/j.earscirev.2010.07.001.

Coffin, M.F., and Eldholm, O., 1994, Large igneous provinces: Crustal structure, dimensions, and external consequences: Reviews of Geophysics, v. 32, p. 1–36, doi:10.1029/93RG02508.

Den, N., Ludwig, W.J., Murauchi, S., Ewing, J.I., Hotta, H., Edgar, N.T., Yoshii, T., Asanuma, T., Hagiwara, K., Sato, T., and Ando, S., 1969, Seismic refraction measurements in the northwest Pacific Basin: Journal of Geophysical Research, v. 74, p. 1421–1434, doi:10.1029/JB074i006p01421.

Dieterich, J.H., 1988, Growth and persistence of Hawaiian volcanic rift zones: Journal of Geophysical Research, v. 93, p. 4258–4270, doi:10.1029/JB093iB05p04258.

Duncan, R.A., and Richards, M.A., 1991, Hotspots, mantle plumes, flood basalts, and true polar wander: Reviews of Geophysics, v. 29, p. 31–50, doi:10.1029/90RG02372.

Fitton, J.G., Mahoney, J.J., Wallace, P.J., and Saunders, A.D., 2004, Leg 192 synthesis: Origin and evolution of the Ontong Java Plateau, *in* Fitton, J.G., Mahoney, J.J., Wallace, P.J., and Saunders, A.D. eds., Proceedings of the Ocean Drilling Program, Scientific Results, Volume 192: College Station, Texas, Ocean Drilling Program, doi:10.2973/odp.proc.sr.192.101.2004.

Foulger, G.R., 2007, The "plate" model for the genesis of melting anomalies, *in* Foulger, G.R., and Jurdy, D.H., eds., Plates, Plumes, and Planetary Processes: Geological Society of America Special Paper 430, p. 1–28, doi:10.1130/2007.2439(1).

Gettrust, J.F., Furukawa, K., and Kroenke, L.W., 1980, Crustal structure of the Shatsky Rise from seismic refraction measurements: Journal of Geophysical Research, v. 85, p. 5411–5415, doi:10.1029/JB085iB10p05411.

Gradstein, F.M., Ogg, J.G., and Smith, A.G., 2004, A Geologic Time Scale: Cambridge, UK, Cambridge University Press, 610 p.

Hilde, T.W., Isezaki, C.N., and Wageman, J.M., 1976, Mesozoic seafloor spreading in the north central Pacific, *in* Sutton, G.H., Manghnani, M.H., Moberly, R., and McAfee, E.U., eds., The Geophysics of the Pacific Ocean Basin and Its Margin: American Geophysical Union Geophysical Monograph 19, p. 205–226, doi:10.1029/GM019p0205.

Houtz, R.E., and Ludwig, W.J., 1979, Distribution of reverberant subbottom layers in the southwest Pacific basin: Journal of Geophysical Research, v. 84, p. 3497–3504, doi:10.1029/JB084iB07p03497.

Ingle, S., and Coffin, M.F., 2004, Impact origin for greater Ontong Java Plateau: Earth and Planetary Science Letters, v. 218, p. 123–134, doi:10.1016/S0012-821X(03)00629-0.

Inoue, H., Coffin, M.F., Nakamura, Y., Mochizuki, K., and Kroenke, L.W., 2008, Intra-basement reflections of the Ontong Java Plateau: Implications for plateau construction: Geochemistry, Geophysics, Geosystems, v. 9, Q04014, doi:10.1029/2007GC001780.

Ito, G., and Clift, P.D., 1998, Subsidence and growth of Pacific Cretaceous plateaus: Earth and Planetary Science Letters, v. 161, p. 85–100, doi:10.1016/S0012-821X(98)00139-3.

Jerram, D.W., and Widdowson, M., 2005, The anatomy of continental flood basalt provinces: Geological constraints on the processes and products of flood volcanism: Lithos, v. 79, p. 385–405, doi:10.1016/j.lithos.2004.09.009.

Karp, B.Y., and Prokudin, V.G., 1985, The structure of the sedimentary layer on the Shatsky Rise according to seismic data: Tikhookkean Geology, v. 3, p. 26–33.

Khankishiyeva, L.M., 1989, The structure and seismostratigraphy of the sedimentary cover on the Shatsky Rise (Pacific Ocean): Okeanologiya, v. 29, p. 178–183.

Klaus, A., and Sager, W.W., 2002, Data report: High-resolution site survey seismic reflection data for ODP Leg 198 drilling on Shatsky Rise, northwest Pacific, *in* Bralower, T.J., Premoli Silva, I., Malone, M.J., et al., Proceedings of the Ocean Drilling Program, Initial Reports, Volume 198: College Station, Texas, Ocean Drilling Program, p. 1–21, doi:10.2973/odp.proc.ir.198.111.2002.

Koppers, A.A.P., Sano, T., Natland, J.H., Widdowson, M., Almeev, R., Greene, A.R., Murphy, D.T., Delacour, A., Miyoshi, M., Shimizu, K., Li, S., Hirono, N., and Geldmacher, J., and the Expedition 324 Scientists, 2010, Massive basalt flows on the southern flank of Tamu Massif, Shatsky Rise: A reappraisal of ODP Site 1213 basement units, *in* Sager, W.W., Sano, T., Geldmacher, J., and the Expedition 324 Scientists, Proceedings of the Integrated Ocean Drilling Program, Volume 324: Tokyo, Integrated Ocean Drilling Program Management International, Inc., doi:10.2204/iodp.proc.324.109.2010.

Korenaga, J., 2005, Why did not the Ontong Java Plateau form subaerially?: Earth and Planetary Science Letters, v. 234, p. 385–399, doi:10.1016/j.epsl.2005.03.011.

Korenaga, J., and Sager, W.W., 2012, Seismic tomography of Shatsky Rise by adaptive importance sampling: Journal of Geophysical Research, v. 117, B08102, doi:10.1029/2012JB009248.

Larson, R.L., and Chase, C.G., 1972, Late Mesozoic evolution of the western Pacific Ocean: Geological Society of America Bulletin, v. 83, p. 3627–3644, doi:10.1130/0016-7606(1972)83[3627:LMEOTW]2.0.CO;2.

Ludwig, W.J., and Houtz, R.E., 1979, Isopach map of sediments in the Pacific Ocean basin and marginal sea basins: Tulsa, Oklahoma, American Association of Petroleum Geologists, 2 sheets.

MacDonald, G.A., 1972, Volcanoes: Englewood Cliffs, New Jersey, Prentice Hall, Inc., 510 p.

Macdonald, G.A., and Abbott, A.T., 1970, Volcanoes in the Sea: Honolulu, University of Hawaii Press, 441 p.

Mahoney, J.J., and Spencer, K.J., 1991, Isotopic evidence for the origin of the Manihiki and Ontong Java oceanic plateaus: Earth and Planetary Science Letters, v. 104, p. 196–210, doi:10.1016/0012-821X(91)90204-U.

Mahoney, J.J., Duncan, R.A., Tejada, M.L.G., Sager, W.W., and Bralower, T.J., 2005, Jurassic-Cretaceous boundary age and mid-ocean ridge type mantle source for Shatsky Rise: Geology, v. 33, p. 185–188, doi:10.1130/G21378.1.

Mitchum, R.M., Jr., Vail, P.R., and Sangree, J.B., 1977, Seismic stratigraphy and global changes in sea level, Part 6: Stratigraphic interpretation of seismic reflection patterns in depositional sequences, *in* Payton, C.E., ed., Seismic Stratigraphy—Applications to hydrocarbon exploration: American Association of Petroleum Geologists Memoir 26, p. 117–143.

Mutter, J.C., 1985, Seaward dipping reflectors and the continent-ocean boundary at passive continental margins: Tectonophysics, v. 114, p. 117–131, doi:10.1016/0040-1951(85)90009-5.

Nakanishi, M., Sager, W.W., and Klaus, A., 1999, Magnetic lineations within Shatsky Rise, northwest Pacific Ocean: Implications for hot spot-triple junction interaction and oceanic plateau formation: Journal of Geophysical Research, v. 104, p. 7539–7556, doi:10.1029/1999JB900002.

Nakanishi, M., Sager, W.W., and Korenaga, J., this volume, Reorganization of the Pacific-Izanagi-Farallon triple junction in the Late Jurassic: Tectonic events before the formation of the Shatsky Rise, *in* Neal, C.R., Sager, W.W., Sano, T., and Erba, E., eds., The Origin, Evolution, and Environmental Impact of Oceanic Large Igneous Provinces: Geological Society of America Special Paper 511, doi:10.1130/2015.2511(05).

Planke, S., and Eldholm, O., 1994, Seismic response and construction of seaward dipping wedges of flood basalts: Vøring volcanic margin: Journal of Geophysical Research, v. 99, p. 9263–9278, doi:10.1029/94JB00468.

Planke, S., Symonds, P.A., Alvestad, E., and Skogseid, J., 2000, Seismic volcanostratigraphy of large-volume basaltic extrusive complexes on rifted margins: Journal of Geophysical Research, v. 105, p. 19,335–19,351, doi:10.1029/1999JB900005.

Richards, M.A., Duncan, R.A., and Courtillot, V.E., 1989, Flood basalts and hot-spot tracks: Plume heads and tails: Science, v. 246, p. 103–107, doi:10.1126/science.246.4926.103.

Ridley, V.A., and Richards, M.A., 2010, Deep crustal structure beneath large igneous provinces and the petrologic evolution of flood basalt: Geochemistry, Geophysics, Geosystems, v. 11, Q09006, doi:10.1029/2009GC002935.

Rogers, G.C., 1982, Oceanic plateau as meteorite impact signatures: Nature, v. 299, p. 341–342, doi:10.1038/299341a0.

Rossi, M.J., 1996, Morphology and mechanism of eruption of postglacial shield volcanoes in Iceland: Bulletin of Volcanology, v. 57, p. 530–540, doi:10.1007/BF00304437.

Rotstein, Y., Schlich, R., and Munschy, M., 1992, Structure and tectonic history of the southern Kerguelen Plateau (Indian Ocean) deduced from seismic reflection data: Tectonics, v. 11, p. 1332–1347, doi:10.1029/91TC02909.

Rutten, M.G., 1964, Formation of a plateau basalt series (from the example of Iceland): Bulletin of Volcanology, v. 27, p. 93–111, doi:10.1007/BF02597514.

Sager, W.W., 2005, What built Shatsky Rise, a mantle plume or ridge tectonics?, *in* Foulger, G.R., Natland, J.H., Presnall, D.C., and Anderson, D.L., eds., Plates, Plumes, and Paradigms: Geological Society of America Special Paper 388, p. 721–733, doi:10.1130/0-8137-2388-4.721.

Sager, W.W., and Han, H.-C., 1993, Rapid formation of Shatsky Rise oceanic plateau inferred from its magnetic anomaly: Nature, v. 364, p. 610–613, doi:10.1038/364610a0.

Sager, W.W., Kim, J., Klaus, A., Nakanishi, M., and Khankishieva, L.M., 1999, Bathymetry of Shatsky Rise, northwest Pacific Ocean: Implications for ocean plateau development at a triple junction: Journal of Geophysical Research, v. 104, p. 7557–7576, doi:10.1029/1998JB900009.

Sager, W.W., Sano, T., and Geldmacher, J., and the Expedition 324 Scientists, 2010, Proceedings of the Integrated Ocean Drilling Program, Volume 324: Tokyo, Integrated Ocean Drilling Program Management International, Inc., doi:10.2204/iodp.ir.324.2010.

Sager, W.W., Sano, T., and Geldmacher, J., 2011, How do oceanic plateaus form? Clues from drilling at Shatsky Rise: Eos (Transactions, American Geophysical Union), v. 92, p. 37–44, doi:10.1029/2011EO050001.

Sager, W.W., Zhang, J., Korenaga, J., Sano, T., Koppers, A.A.P., Mahoney, J., and Widdowson, M., 2013, An immense shield volcano within Shatsky Rise oceanic plateau, northwest Pacific Ocean: Nature Geoscience, v. 6, p. 976–981, doi:10.1038/ngeo1934.

Saunders, A.D., 2005, Large igneous provinces: Origin and environmental consequences: Elements, v. 1, p. 259–263, doi:10.2113/gselements.1.5.259.

Shipboard Scientific Party, 2002, Site 1213, *in* Bralower, T.J., Premoli Silva, I., Malone, M.J., et al., Proceedings of the Ocean Drilling Program, Initial Reports, Volume 198: College Station, Texas, Ocean Drilling Program, 110 p., doi:10.2973/odp.proc.ir.198.109.2002.

Sigmundsson, F., 2005, Iceland Geodynamics: Crustal Deformation and Divergent Plate Tectonics: Berlin, Springer, 214 p.

Sliter, W.V., and Brown, G.R., 1993, Shatsky Rise: Seismic stratigraphy and sedimentary record of Pacific paleoceanography since the Early Cretaceous, *in* Natland, J.H., Storms, M.A., et al., eds., Proceedings of the Ocean Drilling Program, Scientific Results, Volume 132: College Station, Texas, Ocean Drilling Program, doi:10.2973/odp.proc.sr.132.302.1993.

Smith, D.K., 1988, Shape analysis of Pacific seamounts: Earth and Planetary Science Letters, v. 90, p. 457–466.

Smith, W.H.F., and Sandwell, D.T., 1997, Global seafloor topography from satellite altimetry and ship depth soundings: Evidence for stochastic reheating of the oceanic lithosphere: Science, v. 277, p. 1956–1962, doi:10.1126/science.277.5334.1956.

Spitzer, R., White, R.S., Christie, P.A.F., and the iSIMM Team, 2008, Seismic characterization of basalt flows from the Faroes margin and the Faroe-Shetland basin: Geophysical Prospecting, v. 56, p. 21–31, doi:10.1111/j.1365-2478.2007.00666.x.

Tryggvason, E., and Bath, M., 1961, Upper crustal structure of Iceland: Journal of Geophysical Research, v. 66, p. 1913–1925, doi:10.1029/JZ066i006p01913.

Uenzelmann-Neben, G., Gohl, K., Ehrhart, A., and Seargent, M., 1999, Agulhas Plateau, SW Indian Ocean: New evidence for excessive volcanism: Geophysical Research Letters, v. 26, p. 1941–1944, doi:10.1029/1999GL900391.

Vuong, A.K., Zhang, J., Gibson, R.L., Jr., and Sager, W.W., this volume, Application of the two-dimensional continuous wavelet transforms to imaging of the Shatsky Rise plateau using marine seismic data, *in* Neal, C.R., Sager, W.W., Sano, T., and Erba, E., eds., The Origin, Evolution, and Environmental Impact of Oceanic Large Igneous Provinces: Geological Society of America Special Paper 511, doi:10.1130/2015.2511(07).

Walker, G.P.L., 2000, Basaltic volcanoes and volcanic systems, *in* Sigurdsson, H., Houghton, B., Rymer, H., Stix, J., and McNutt, S., eds., Encyclopedia of Volcanoes: San Diego, California, Academic Press, p. 283–289.

Manuscript Accepted by the Society 23 December 2014
Manuscript Published Online 24 March 2015

Geological Society of America Special Papers

The Shatsky Rise oceanic plateau structure from two-dimensional multichannel seismic reflection profiles and implications for oceanic plateau formation

Jinchang Zhang, William W. Sager and Jun Korenaga

Geological Society of America Special Papers 2015;511; 103-126 , originally published onlineMarch 24, 2015
doi:10.1130/2015.2511(06)

Notes